A STUDY OF COLLAPSE EVENTS IN ULTRAVIOLET LIGHT FILAMENTS
DUE TO TRANSIENT EDGE EFFECTS

THESIS

Paul L. Muller, Captain, USAF

AFIT/GAP/ENP/06-12

DEPARTMENT OF THE AIR FORCE
AIR UNIVERSITY

AIR FORCE INSTITUTE OF TECHNOLOGY

Wright-Patterson Air Force Base, Ohio

AFIT/GAP/ENP/06-12

A STUDY OF COLLAPSE EVENTS IN ULTRAVIOLET LIGHT FILAMENTS

DUE TO TRANSIENT EDGE EFFECTS

THESIS

Presented to the Faculty

Department of Engineering Physics

Graduate School of Engineering and Management

Air Force Institute of Technology

Air University

Air Education and Training Command

In Partial Fulfillment of the Requirements for the

Degree of Master of Science (Applied Physics)

Paul L. Muller, BS

Captain, USAF

March 2006

A STUDY OF COLLAPSE EVENTS IN ULTRAVIOLET LIGHT FILAMENTS DUE TO TRANSIENT EDGE EFFECTS

Paul L. Muller, BS
Captain, USAF

Approved:
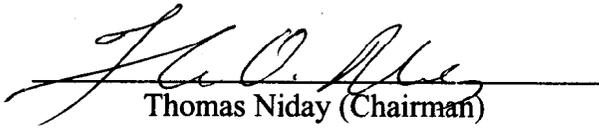
_____   9 Mar 06
Thomas Niday (Chairman)   date

_____   9 Mar 06
Matthew Bohn (Member)   date

_____   9 Mar 06
David Weeks (Member)   date

AFIT/GAP/ENP/06-12

Abstract

Intense, short light pulses can form filaments capable of propagating kilometers through the atmosphere. This is due to the nonlinear index of refraction of the atmosphere in response to the pulse's high intensity, which creates a self-focusing effect that further intensifies the pulse. This focusing is balanced by the formation of defocusing plasma by the pulse. A split-step propagation model was used to simulate the propagation of these pulses through the atmosphere and investigate the collapse of long ultraviolet pulses of 10-100 picoseconds in duration due to transient edge effects. The structures of individual collapse events in the pulse were characterized. The pulses collapsed linearly, yet independently of the initial pulse power. The number of collapses the pulse undergoes scaled with the initial power, and the plasma decay rate was found to dictate collapse event spacing. Additional collapses on the trailing edge of the pulse were also observed, and may have been created by the pulse field overflowing the grid used to model the propagation. Group velocity dispersion was included to add capabilities to model short pulses in the ultraviolet. Short pulses of 100 femtoseconds or less were observed to collapse in a manner similar to the longer pulses.

Acknowledgments

I would like to express my sincere appreciation to my faculty advisor, Capt. Thomas Niday, for his guidance throughout the course of this thesis effort. I would also like to thank my wife for keeping me mostly sane during my time at AFIT and while working on this thesis.

Paul L. Muller

Table of Contents

List of Figures

A STUDY OF COLLAPSE EVENTS IN ULTRAVIOLET LIGHT FILAMENTS DUE TO TRANSIENT EDGE EFFECTS

I. Introduction

Background

Remote sensing protects the user from harmful environmental effects, allows him reach to denied areas, and shields him from exposure to enemy sensing capabilities. Remote sensing technologies such as light detection and ranging (LIDAR) based on long-path absorption methods including Fourier-transform infrared spectroscopy and differential optical absorption spectroscopy are constrained by their light sources [1, 2]. These sources are limited by their inability to propagate over long paths or through atmospheric obscurations such as rain, clouds, and turbulence, and to operate on multiple wavelengths simultaneously [1, 3]. Finding ways to increase sensor range is crucial in extending sensor capabilities and increasing the safety of the user. The study of the propagation of ultra-short light pulses or filaments holds promise in overcoming range limitations of current remote sensor systems.

Short, intense light pulses introduce a nonlinear self-focusing effect that aids in long distance propagation by changing the refractive index of the surrounding air [4, 5, 6, 7]. Low-intensity laser pulses diffract as they pass through the atmosphere, resulting in unwanted scattering and yielding low intensities on the target. If a pulse is sufficiently short and high enough in peak power, a nonlinear self-focusing effect will cause the pulse to intensify, overcome diffraction, and in turn focus tighter as it propagates, which will further intensify the beam [7, 8]. This nonlinear Kerr effect, or intensity dependent refractive index occurs above a certain critical power and creates a focusing lens in the refractive profile of the air [9]. When the pulse reaches a certain intensity, it ionizes the air, forming plasma. The presence of plasma causes two processes to occur – it absorbs photons from the pulse and changes the refractive index of the air, defocusing the pulse, which reduces the index of refraction as the pulse intensity diminishes [1, 10]. If the focusing and defocusing effects are balanced, the pulse can form a filament that is capable of propagating over long distances and possibly through atmospheric turbulence and scattering bodies such as clouds or aerosols much more effectively than a continuous wave (CW) beam or low intensity pulse could [1, 11].

As the pulse temporally compresses and self-phase modulates it can generate a white light supercontinuum [1, 8, 11] that could be used in spectroscopic techniques for detecting chemicals or bio-agents present in the air. This continuum of light ranges from the ultraviolet to the infrared in wavelength. By creating this supercontinuum and directing it at targets such as airborne particles, aerosols, or gaseous clouds, remote spectroscopy could be possible by observing the absorption of certain wavelengths or emitted lines by the material under inspection. This could lead to increased standoff

distances for existing sensors as well as increased safety in detecting possible chemical-biological threats in the field. In addition, the plasma channels created by the filaments could be used to control an electrical discharge such as lightning [1, 12, 13, 14]. Filaments could also be used for long-range (1 km or more) ablation of materials for spectroscopic purposes [5, 15]. Therefore, many applications for these filaments exist in the field of remote sensing.

The high intensity required to create each filament induces a self-phase modulation, which leads to the broadband white light continuum being created [1, 11, 12]. This white light can be useful in applications where a broad range of wavelengths are needed, and the long distances these white light pulses are capable of traveling open up new possibilities for spectroscopy [1, 2, 10, 16]. There has been significant work done in modeling and observing the propagation of filaments through the atmosphere with emphasis on using it for spectroscopy [2]. Kasparian *et al.* are using a mobile femtosecond pulse generator known as the Teramobile for generating white-light filaments for atmospheric analysis purposes using lasers in the infrared (IR) range [1]. Current LIDAR techniques are limited to single wavelengths, which can make spectroscopy tedious because only one wavelength can be examined at a time, and a large scan of wavelengths may be required before one interacts with the target of interest in a meaningful way [1, 2]. By including all wavelengths at once in a LIDAR pulse, spectroscopy could become much more efficient. The Teramobile team hopes to utilize these white light pulses over long distances in the atmosphere (several kilometers) to perform spectroscopy on pollutants and other substances present in the air [1]. The same

3

technique could be applied for military applications to areas with supposed chemical or biological contamination, or on remote targets of interest such as vehicles.

Modeling work done with the interaction of light filaments with aerosol obscurants [17] will be useful in determining the feasibility of atmospheric spectroscopy and the use of filaments in propagating through a cloud of chemical or biological obscurants in the air. For powers much larger than the critical power required to create a filament, instability can cause the initial pulse to break up into several spots during the self-focusing process [18]. These pieces can propagate as a parallel bundle of filaments, and vanish and reappear as they travel [1, 4, 18]. They may also self-heal and form a single filament as they propagate [18]. A benefit of this instability is that if the filament encounters an obscurant such as an aerosol, the filament may still be able to propagate after it has split into several pieces, and eventually recombine into a single filament with little loss of energy [17, 18]. Early simulations have shown that this occurs with a 10-15% loss in power [17]. This shows promise in the possibility of propagation through a cloud of obscurants, and insuring that enough power remains in the filament to be of use in long range sensing.

Problem Statement

While many studies and experiments concerning light filaments have concentrated on the infrared region of the spectrum, the ultraviolet (UV) region offers lower peak powers required to generate pulses of sufficient intensity to cause self-focusing effects, as well as the ability to use longer pulses, on the order of picoseconds rather than the femtosecond scale. However, current long pulse filament models in the

ultraviolet exhibit spatial and temporal instabilities in the pulse that limit the propagation distance due to collapse, as well as edge effects that consume the pulse as it propagates [19]. In Niday's model, the initial collapse event that forms on the leading edge of the pulse leads to non-physical results in modeling further pulse propagation and collapse events due to the extremely high intensities and plasma levels output by the model in a very small region of space. Finding ways to stabilize the propagation of the pulse and understand the collapse events taking place would serve to strengthen the code and validate its output in a meaningful, physical way. The main goal of this project was to gain a deeper understanding of collapse events that consume the leading edge of the pulse due to edge effects, and to determine if there are initial physical characteristics that can be used when generating the pulse in the model that will eliminate or minimize this collapse. Efforts to understand and characterize the collapse events were constrained to the ultraviolet region.

Research Objectives/Focus

Figure 1.1 shows the breakdown of a finite pulse as the instabilities of the pulse edges cause it to collapse as generated by Niday's filament propagation code [19]. The pulse modeled is 400 ps in duration and has 500 MW of initial peak power. It was also initially seeded with noise, which contributes to the modulational instability that leads to the collapse of the pulse. The leading edge of the pulse is also undergoing a series of collapses, which is an additional cause of the inability of the pulse to propagate long distances. Determining a relationship between beam characteristics and the way the edge effects cause the beam to collapse was the focus of the project. In order to achieve larger

5

propagation ranges, this instability in pulse propagation needs to be addressed. Propagation distances of several Rayleigh ranges are considered to be long distances when compared to a standard Gaussian beam [1]. This is due to the low number of photons required to ionize air when operating in the UV range, which absorbs energy quickly from the pulse as it propagates through the atmosphere.

Niday came to several conclusions in his study of UV long pulse propagation [19]. First, the collapse events on the leading edge of the pulse are due to the transient shape of the edge of the pulse, which does not match a steady state solution. While results indicated that the pulse may still collapse regardless of the initial pulse shape, a supergaussian shape was chosen because it emulates a steady state solution in the middle of the pulse, while still retaining edges. Because the edges are not flat (i.e., steady state) like the rest of the pulse, they begin to break down and collapse. The plasma created by these pulses causes a dip in the field, which forms a ring and seeds the next collapse. This occurs because the pulse is attempting to move towards a steady state solution.
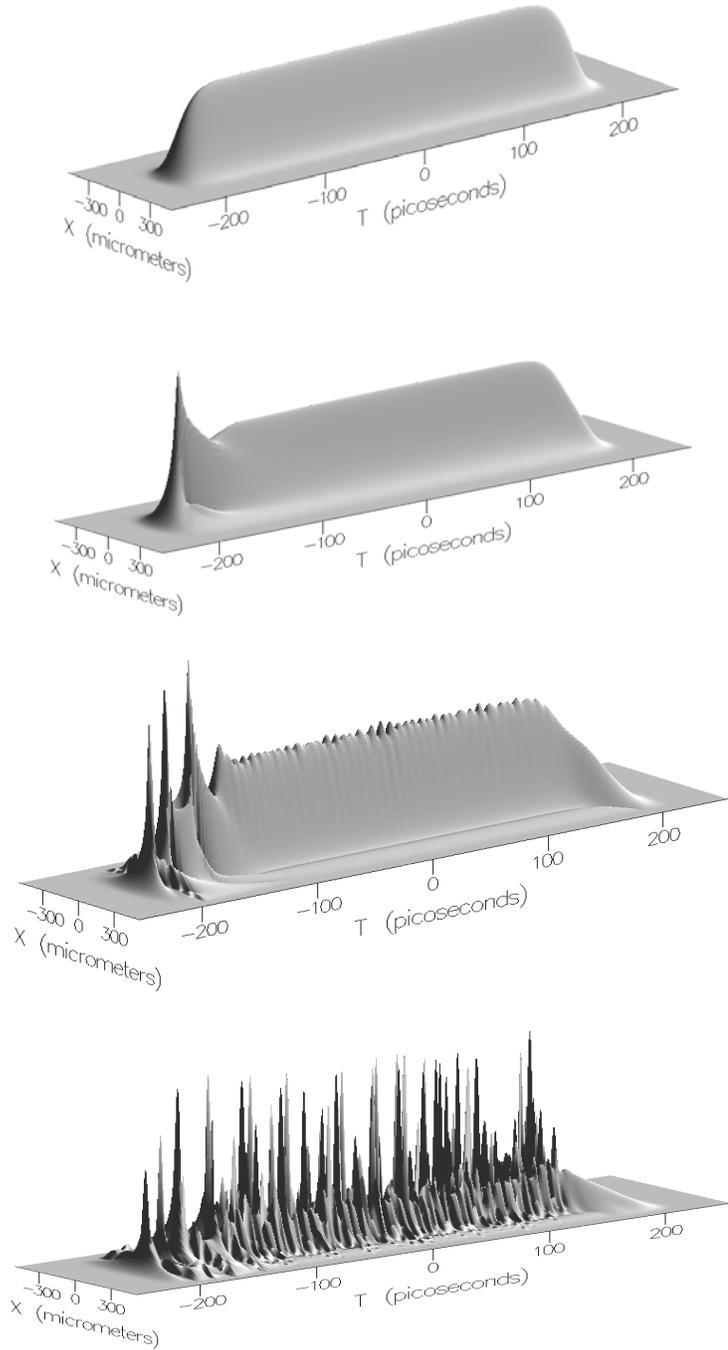
Figure 1.1: Propagation of a 400 ps, 500 MW finite pulse illustrating how edge effects and modulational instability causes a complete collapse in time. These effects limit the ability of the pulse to travel distances over a few centimeters as a filament in the current model. The pulse is shown at varying values of *z*, or distance of propagation that the pulse has traveled. The T axis refers to the pulse duration, the X axis is the pulse width, and the Z axis (not labeled) is the relative amplitude of the pulse in arbitrary units. Reproduced, with permission, from Niday [19].

7

Niday also stated that the collapse events themselves seem to consume the pulse at a linear rate [19]. That is, they do not become more rapid as more of the pulse is consumed. The shape and spacing of the collapsed peaks seems to be defined by the numerical parameters of the model grid. Studies done to check the convergence of these collapse peaks in time were not able to completely resolve the peaks for long pulses, so their exact shape is not known. More information is required about these individual collapse events, including their creation, shape and spacing. These observations served as a starting point in the attempt to more fully understand why the pulses collapse and what could be done to prevent this from happening, or at least mitigate the collapse.

Methodology

This project is based on prior work completed by Niday [19] and his simulation of filament propagation in the UV range. He created a filament propagation model in Fortran 90 along with a graphical user-interface (GUI) in OpenGL. Niday's work was based on studies and simulations conducted by Schwarz and Diels [20]. These two previous works are the basis for studying the characteristics of long pulse filament propagation in the UV using numerical modeling techniques. The results of these studies still leave room for many areas to be investigated, such as the collapse of the pulses after a certain time period due to transient edge effects, and the effects of varying physical and numerical parameters within the models.

The propagation of UV light filaments was modeled by a numerical split-step spectral technique [19, 21]. The model was used to generate results and altered to more fully understand the collapse events that the pulses undergo as they travel through the

atmosphere. In addition, the model was made more sophisticated to allow for variations on the filament being studied including studying short pulses of the length traditionally studied in the IR. Numerical and physical parameters of the model were varied in an effort to mitigate the collapse of the pulse, and reasons for the creation and spacing of the collapse events were determined.

The collapse events were shown to be independent of the initial peak power of the pulse, and the leading edge collapses would consume the pulse at a linear rate. The number of collapse events generated varied with the initial peak power, as a higher power pulse could generate collapses more rapidly, and the spacing between each collapse event was limited by the decay rate of the plasma once the pulse had dropped in intensity to such a degree that the plasma was no longer able to be sustained. In addition, the addition of group velocity dispersion and an attempt to model shorter UV pulses with durations of 10 -100 fs resulted in the collapse of the pulses very similar to the collapse of the long (>1 ps) pulses.

II. Literature Review

Chapter Overview

This chapter addresses the equations that form the basis of modeling pulse propagation and introduces several physical characteristics such as the nonlinear index of refraction, group velocity dispersion, and the plasma that balances the focusing effects during filament propagation. It also covers the numerical model used to simulate pulse propagation and existing issues with this model that were studied during the project.

Propagation Equation

Starting with the Maxwell wave equation and including a nonlinear polarization term, Schwarz and Diels [20] and Niday [19] add the effects of plasma generated by the pulse and obtain a propagation equation as such:

$$
\begin{aligned}
\frac{\partial \mathcal{E}}{\partial z} = &\frac{i}{2k} \nabla_\perp^2 \mathcal{E} - \frac{ik^{''}}{2} \frac{\partial^2 \mathcal{E}}{\partial t^2} - \frac{\beta^{(K)}}{2} |\mathcal{E}|^{2K-2} \mathcal{E} \\
&- \frac{\sigma}{2}(1+i\omega\tau)\rho\mathcal{E} + ik_0 n_2 |\mathcal{E}|^2 \mathcal{E} + ik_0 n_2 \left[\int_{-\infty}^{\infty} dt' R(t-t') |\mathcal{E}(t')|^2 \right] \mathcal{E}
\end{aligned}
\tag{2.1}
$$

Under certain conditions, this equation can be reduced to the nonlinear Schrödinger equation, so it is sometimes referred to by that name. Here, $\mathcal{E}$ is the complex amplitude, or slowly varying envelope of the real electric field, E, and has units of intensity such that $|\mathcal{E}|^2$ is the intensity in W/m^2. $\mathcal{E}$ is related to the electric field by

$$
E(x,y,z,t) = \frac{1}{2} \mathcal{E}(x,y,z,t) e^{i(kz-\omega t)} + c.c.
\tag{2.2}
$$

where *c.c.* is the complex conjugate [19]. Equation 2.1 describes how $\mathcal{E}$ changes as a function of the propagation distance, *z*. On the right side of the equation, the first term

represents transverse diffraction where k is a wave number, the second term describes group velocity dispersion where k'' is the group velocity dispersion coefficient, and the third term is loss due to multi-photon ionization (MPI) generation, where $\beta^{(K)}$ is the MPI coefficient at order K. The fourth term is a plasma defocusing and absorption term where σ is the cross section for inverse bremsstrahlung, ω is the optical reference frequency of the light, τ is the electron collision time, and ρ is the electron plasma density. The next two terms describe the self-focusing, with the final term in the equation describing the Raman effect, which is important if the time scale of the pulse is such that the nonlinear refractive index term n_2 can not be assumed to be instantaneous.

The electron density of the plasma is a time-dependent quantity described as

$$\frac{\partial \rho}{\partial t} = C\rho|\mathcal{E}|^2 + \frac{\beta^{(K)}|\mathcal{E}|^{2K}}{K\hbar\omega} - \alpha\rho^2 + D\nabla_\perp^2\rho \qquad (2.3)$$

where C is a coefficient for avalanche ionization, α is an electron-positive ion recombination coefficient, and D is diffusion strength. For pulses less than tens of nanoseconds, C can be neglected [20] because the time scale of the pulse is such that C does not have time to effect the pulse before the pulse has moved on in space. For pulses long enough that the plasma can reach a steady state, $\frac{\partial \rho}{\partial t} = 0$. Long UV pulses are on the order of a hundred or more picoseconds, which is short enough to neglect C but long enough that the plasma can reach steady state, as the temporal duration of the pulse is much longer than the response (rate of change) of the plasma. Neglecting the diffusion term as well gives a steady state plasma density that is the solution of a quadratic equation at each point in space [19].

11

Equation 2.1 is used as the basis for simulating the propagation of the light pulse through the atmosphere using numerical computational techniques. Some numerical propagation models [19, 20] neglect group velocity dispersion (GVD) and let the self-focusing term be instantaneous by not including the Raman effect. These approximations, along with a steady state plasma solution cause Equation 2.1 to become time-independent and reduce it to

$$\frac{\partial \mathcal{E}}{\partial z} = \frac{i}{2k}\nabla_{\perp}^{2}\mathcal{E} - \frac{\beta^{(K)}}{2}|\mathcal{E}|^{2K-2}\mathcal{E} - \frac{\sigma}{2}(1+i\omega\tau)\rho\mathcal{E} + ik_{0}n_{2}|\mathcal{E}|^{2}\mathcal{E}. \tag{2.4}$$

GVD is evident in the propagation of pulses with durations several orders of magnitude smaller than the 100 ps pulses dealt with in the model. Therefore, it is possible to neglect it initially because the code is dealing with either continuous wave (CW) beams, or long pulses on the order of hundreds of picoseconds. GVD typically does not have an effect on pulse propagation unless the time scale is 100 femtoseconds or less, because the large spectral content of the pulses cause shorter pulses to be more affected by GVD. This topic will be covered further in Chapter 3.

The plasma can also be modeled in another, time-independent way. Schwarz and Diels make the plasma term an effective n_3 term [19, 20] and neglect MPI generation, which changes the form of Equation 2.4 slightly to

$$\frac{\partial \mathcal{E}}{\partial z} = \frac{i}{2k}\nabla_{\perp}^{2}\mathcal{E} + ik_{0}n_{2}|\mathcal{E}|^{2}\mathcal{E} + ik_{0}n_{3}|\mathcal{E}|^{3}\mathcal{E}. \tag{2.5}$$

Here, $k_{0}n_{3}|\mathcal{E}|^{3}$ is equal to the plasma defocusing coefficient $\sigma\omega\tau\rho/2$ in Equation 2.4, and n_3 is equal to

$$-\sqrt{\frac{\sigma^{(3)}N_0}{\alpha}}\,\frac{e^2}{2n_0\omega^2 m_e\varepsilon_0}\,, \tag{2.6}$$

where e is the charge of the electron, ε_0 is the permittivity of free space, and m_e is the mass of an electron [20]. This simplified model allows for a propagation equation that is easier to work with because the plasma equation does not need to be solved as a function of time, and the n_3 value is taken from Schwarz and Diels [20]. Once the propagation equation is in the form of Equation 2.4 or Equation 2.5, it can be used to model the propagation of a pulse using the split operator method, which is covered in the section on numerical modeling. Both Equation 2.4 and Equation 2.5 can be used to study pulse propagation where the pulse is time independent, and will be discussed further in the section covering numerical techniques, though Equation 2.4 is used in this work because it includes the time-dependent plasma term.

Self-Focusing

Several theories exist for the reasoning behind the propagation of these intense light pulses [19]. The self-guiding theory is the case in which the pulse is guided by a balance between the Kerr effect and ionized plasma that creates an effective waveguide in the atmosphere [22]. The moving focus model states that each section of the pulse in time focuses at a different distance along the axis of propagation due to a different peak power, which produces the elongated filament that is observed [8, 22]. Finally, a dynamic spatial replenishment theory hypothesizes that the pulse experiences multiple collapses as it decays in space and is replenished each time by power from the trailing edge of the pulse. The leading edge of the pulse collapses due to self-focusing effects while the

trailing edge of the pulse defocuses due to the plasma created by the leading edge [22, 23]. As propagation continues, the leading edge dissipates from nonlinear absorption present in the plasma, but the trailing edge refocuses and replenishes the pulse intensity. The pulse appears to be one continuous filament, when in fact it is actually several pulses forming and dissipating.

A certain critical power must be reached before self-focusing can occur and a filament can be formed. This critical power is given by

$$P_{crit} = \frac{\lambda^2}{2\pi n_0 n_2} \tag{2.7}$$

where n_0 is the background index and λ is the wavelength [20]. For UV propagation, the critical power is around 125 MW for a wavelength of 248 nm [19]. The propagation distance is equivalent to several times the Rayleigh range [18, 24], which is the distance over which the pulse radius expands by $\sqrt{2}$ and the intensity is halved [22, 24]:

$$z_0 = \pi w_0^2 n_b / \lambda_0, \tag{2.8}$$

where z_0 is the distance from the waist and w_0 is the waist size of the initial pulse. The self-focusing n_2 term causes the field to continually generate a higher index of refraction, leading to a self-focusing collapse of the pulse. This collapse stops once it is balanced by the ionization of air particles by the pulse itself, causing defocusing and losses from the generated plasma. This balance is crucial in the pulse's propagation, because if the collapse continues unbalanced, the plasma it has generated will quickly absorb the pulse and propagation will cease. If the collapse is balanced correctly, the pulse will begin to

14

expand until its intensity is too weak to maintain the plasma, and the plasma is no longer strong enough to stop the collapse, and the process begins again with a new self-collapse.

There are also issues with the length of time over which the plasma is generated versus the distance the filament propagates in space. In the models proposed by Schwarz and Diels [20] and Niday [19], the pulse is taken to be independent of time by assuming that the scale of the pulse, which is typically hundreds of picoseconds in length in the UV, is much greater than the time scale of the nonlinear response of the air as the pulse travels through it [19, 20]. This version of the nonlinear propagation equation is dealing with an effective continuous wave (CW) solution rather than a pulsed beam, which corresponds with the aforementioned self-guiding theory.

Both Schwarz and Diels [20] and Niday [19] studied long pulses in the UV. With long pulses, the plasma is treated as an instantaneous effect and that the time dependence has been removed. This approximation only works if the plasma has enough time to reach a steady state, so the time scale of the pulses must be long enough for this to occur. The upper limit of the time scale is constrained by inverse bremsstrahlung, and is between 4-60 ns [20]. The lower limit is determined by how long the plasma takes to reach a steady state, and is 30-200 ps [20]. Generally, a value of 100 or more picoseconds is used to model a long pulse. This is important because it allows the use of a n_3 term to model the plasma and makes modeling the propagation of the pulse much simpler as a differential or quadratic equation does not need to be used to model the behavior of the plasma as the pulse evolves.

Numerical Techniques for Modeling Propagation

An important issue that should be introduced initially is what is meant by the terms two and three dimensions in the case of the numerical method used to model pulse propagation. The 2D and 3D code model a 2D spatial field, and use a 2D grid (array) to hold the information describing the field. In both cases, the direction of propagation is designated as the z direction, which is the third spatial dimension. Therefore, all three spatial dimensions are represented, but only two are used to describe the field, and therefore are affected by the numerical transformations that the code performs. The model follows the pulse along the z-axis as it propagates in space, staying in a reference frame situated at the beginning of the pulse. This reference frame moves along at the group velocity of the pulse to observe how the pulse evolves at each step of propagation. It is more convenient to talk about the propagation of the pulse in units of distance rather than time, though time can easily be extracted from the distance the pulse has traveled by the relationship

$$z = c\Delta t,$$
(2.9)

where z is the distance traveled along the z axis, c is the speed of light and Δt is the amount of time that has passed. Because c is very large when compared to the size scale of the pulse and spatial grid used to model the field, allowing the pulse to propagate in space as a function of time would result in the pulse immediately going off of the spatial grid. Alternatively, one could increase the grid size used in describing the field, but this would slow the calculations down and reduce the efficiency of the code, or require a grid with very large spatial increments to be used, which is not useful when studying the evolution of pulses that are only tens of microns in size. Again, while both the 2D and 3D

models use three spatial dimensions, in the 2D code only the *x* and *y* dimensions are transformed via a Fast Fourier Transform (FFT) while *z* has a specific value in each propagation step. In the 3D code, the third dimension transformed by the FFT is time, as the plasma evolves over time as described by Equation 2.3, instead of existing as a steady state. This means that for each propagation step, a differential equation must be solved to evolve the plasma, which will be discussed in further detail in the section covering the 3D propagation method.

Fortran 90 was used to numerically model the propagation of a light filament in the UV region using Equation 2.3. A graphical user interface (GUI) created by Niday and written in OpenGL provides real time feedback on the various characteristics of the pulse, including the beam profile in real and frequency space, beam width, and beam profile history [19]. The program allows for both two (2D) and three-dimensional (3D) beam propagation. As stated previously, in the 3D case, the third dimension refers to a temporal dimension rather than a third spatial dimension. While the 2D code is useful for verification of time-independent beam propagation, the 3D case is used to study the observed collapse events on the leading edge of the pulse. The basic methods for solving both of these cases are discussed in the next section.

2D Propagation Method

The 2D code solves the propagation of a CW beam rather than a finite pulse. It only deals with the two spatial dimensions of the field being propagated. Therefore, the 2D method is time independent and allows the use of the simplified n_3 term to model the plasma being generated by the beam. Figure 2.1 gives an example of a 2D beam.
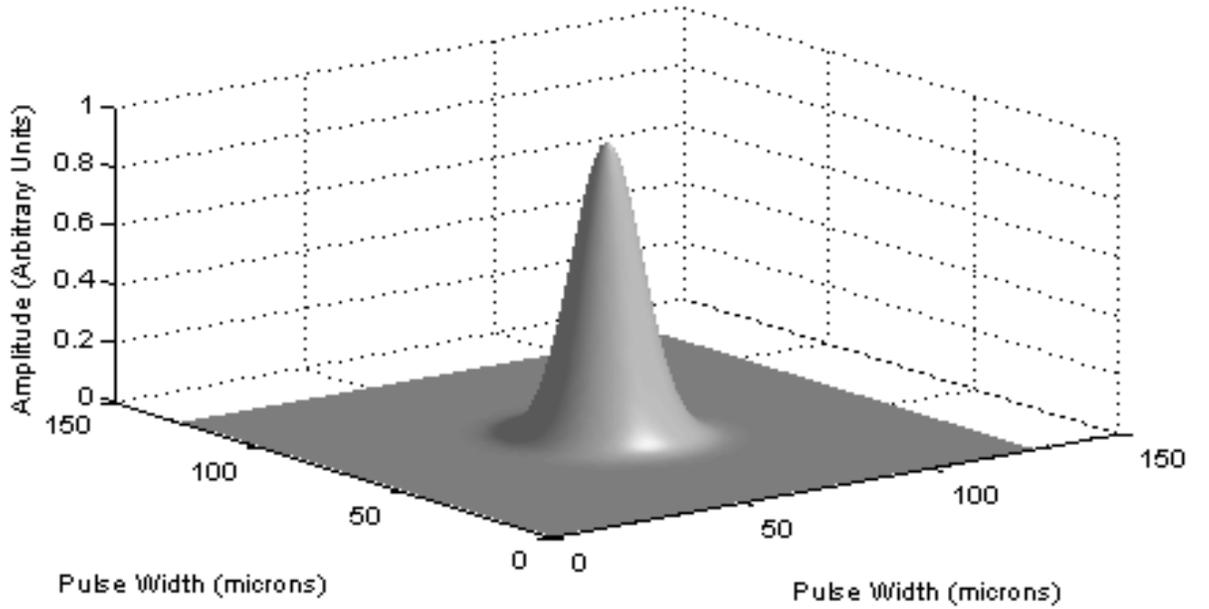
Figure 2.1. Two-dimensional beam shown in both spatial dimensions. This form is utilized in the 2D code to propagate the beam along the third spatial dimension, the *z*-axis.

Starting with the following form of the propagation equation

$$\frac{\partial \mathcal{E}}{\partial z} = \frac{i}{2k} \nabla_{\perp}^2 \mathcal{E} + ik_0 n_2 |\mathcal{E}|^2 \mathcal{E} + ik_0 n_3 |\mathcal{E}|^3 \mathcal{E} + ik_0 n_4 |\mathcal{E}|^4 \mathcal{E}$$
$$- \frac{\beta^{(K)}}{2} |\mathcal{E}|^{2K-2} \mathcal{E} - \frac{\sigma}{2}(1+i\omega\tau)\rho\mathcal{E},$$

(2.10)

a decision based on the numerical modeling method to be used must be made to use

either the n_3 term or the term $\frac{\sigma}{2}(1+i\omega\tau)\rho\mathcal{E}$, depending on how the plasma is to be

modeled. Whichever term is not chosen can be set to zero in the model. Generally, the n_3

term is chosen for simplicity when solving the equation. The split operator method may

then be used to propagate the field in the z direction. This method defines the propagation

operator as two components: a nonlinear index change piece given as

18

$$\hat{V} = k_0 n_2 |\mathcal{E}|^2 + k_0 n_3 |\mathcal{E}|^3 + k_0 n_4 |\mathcal{E}|^4 - \frac{\beta^{(K)}}{2} |\mathcal{E}|^{2K-2} - \frac{\sigma}{2}(1 + i\omega\tau)\rho \qquad (2.11)$$

and a linear diffraction piece given as

$$\hat{T} = \frac{\nabla_\perp^2}{2k_0} \,. \qquad (2.12)$$

Starting with a Gaussian beam as the 2D field, the field may be acted upon with the two operators separately. However, the linear operator is split into two pieces, and the overall operation can be defined as

$$\exp\left(i\frac{\hat{T}\Delta z}{2}\right)\exp\left(i\hat{V}\Delta z\right)\exp\left(i\frac{\hat{T}\Delta z}{2}\right), \qquad (2.13)$$

where each term will operate on the field $\mathcal{E}$ in turn for every step in the z direction, defined by Δz. The method is designated by the name *split* because not only do the two operators not commute, and therefore must be split apart, but also because the $\hat{T}$ operator is split into two parts to minimize the error in the calculations. Because $\hat{T}$ is diagonal in the k space representation, and $\hat{V}$ is diagonal in real space, the field must be transformed using a Fourier transform prior to the first operation, and then transformed back to the spatial representation at the end using another Fourier transform in order to study the behavior of the field in real space as it propagates along z. The Fourier transformations are handled numerically with a FFT routine.

The code first transforms the field to k space to allow half of $\hat{T}$ to operate as the initial step in the split-operator method. Once this is accomplished, another FFT transformation converts the field back to the spatial representation where $\hat{V}$ operates on the field. This is where the nonlinear effects act on the field and the self-focusing occurs.

19

Then, one more transformation back to k space allows the second half of $\hat{T}$ to operate and the process begins again for the next Δz step. This continues until the desired distance along z has been reached, and the field is transformed back into the spatial representation so that the final beam profile can be studied in real space. In the 2D code, a one-dimensional slice of the field is extracted to a new array after every $\hat{V}$ operation so that a beam history can be output to see the evolution of the beam intensity as it propagates along z. Figure 2.2 illustrates how the beam history is recorded and plotted.
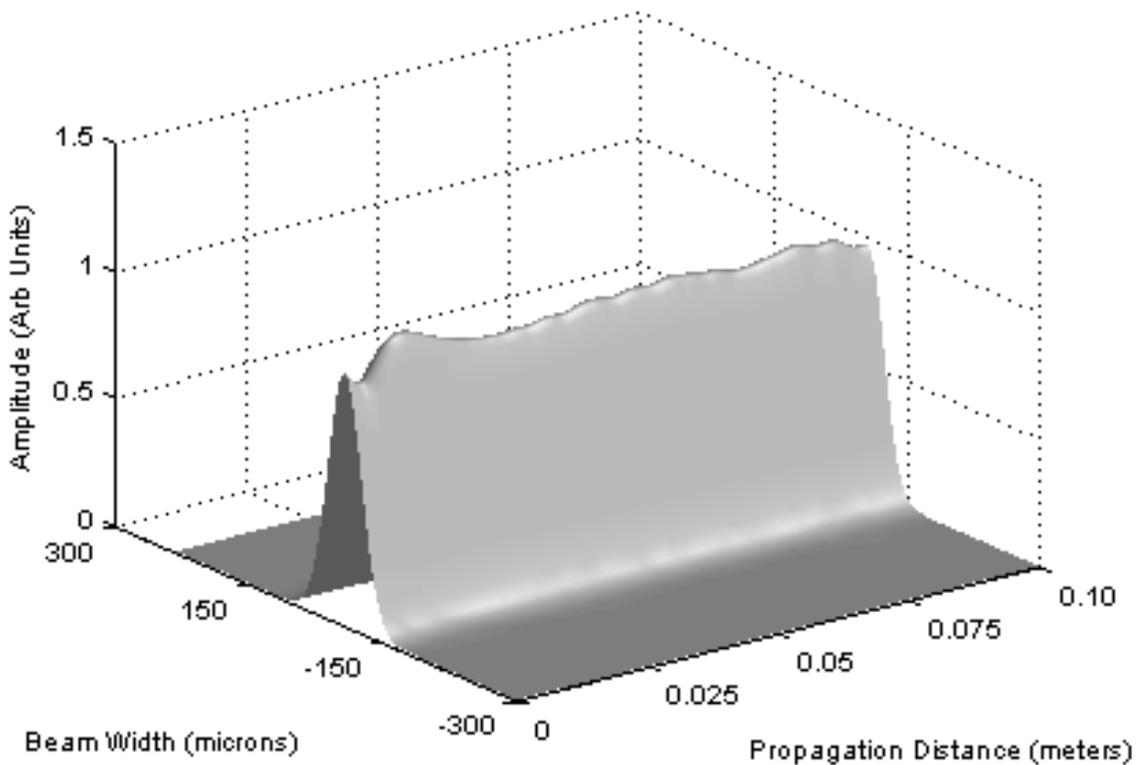
Figure 2.2. History plot of 2D field propagation that shows the evolution of the field as it propagates in the z direction as a function of intensity in arbitrary units. Each z step contains a slice of the field at its maximum value so that focusing and defocusing trends can be easily distinguished.

The main reason for moving between real and frequency space with the split operator method is the way in which derivatives are handled. As is evident in Equation

20

2.10 and the original form of the propagation equation, Equation 2.1, the derivative of the propagating field is calculated in both the spatial and temporal dimensions. However, the code uses no differentiation algorithm to calculate these values; no finite difference method or explicit and separate differentiation routine calculates the derivatives in the model. An inherent property of the Fourier transform is that the derivative of a function $f(x)$ with respect to x is simply the Fourier transform, $F(k)$, multiplied by ik and transformed back to real space via another Fourier transformation. Likewise, a function's derivative with respect to t is accomplished simply multiplying its Fourier transform by $i\omega$ and then transforming back to real space:

$$f^{(j)}(x) = \int_{-\infty}^{\infty} (ik)^j F(k) e^{ikx} dk. \qquad (2.14)$$

A complete, formal treatment of this can be found in Gaskill [25].

3D Propagation Method

The three-dimensional code uses a field that consists of two spatial dimensions defined as x and y, and one time dimension, t. An example is shown in Figure 2.3. The third spatial dimension is still z, the axis along which the pulse propagates, but it is not transformed by the code like the x and y dimensions. A steady state plasma solution is no longer assumed; instead, the differential equation to determine plasma density must be solved:

$$\frac{\partial \rho}{\partial t} = b|\mathcal{E}|^{2K} - a\rho^2. \qquad (2.15)$$

21

In addition, the nonlinear index operator $\hat{V}$ changes because the Schwarz and Diels n_3 term is no longer being used to describe the plasma defocusing effect. The operator now takes the form

$$\hat{V} = k_0 n_2 |\mathcal{E}|^2 - \frac{\beta^{(K)}}{2}|\mathcal{E}|^{2K-2} - \frac{\sigma}{2}(1+i\omega\tau)\rho .$$ (2.16)

The code uses a method based on the exact solution of Equation 2.15 to solve for the plasma density at every x and y value over time [19]. These values are then put back into Equation 2.13 and used to complete the split operator method. The propagation is still accomplished using the split operator method as in the 2D case, but with the new nonlinear index operator and a changing value for the plasma.

The 3D code can compute the evolution of the pulse as a finite pulse or as a section of a CW beam. By using periodic boundary conditions in time, the code treats the pulse as a section of a CW beam. This method is used to study the modulational instability of a section of the pulse as the instability grows [19]. When the pulse is modeled as a finite object, other factors need to be considered, such as the transient edge effects that can also cause the pulse to collapse as it propagates. Because of these edge effects, the pulse can no longer be considered independent of time, as it is not a steady state solution. The issues with both of these types of instabilities seen in Figure 1.1 cause the pulse to collapse. The collapse of the leading edge is the main focus of this project.
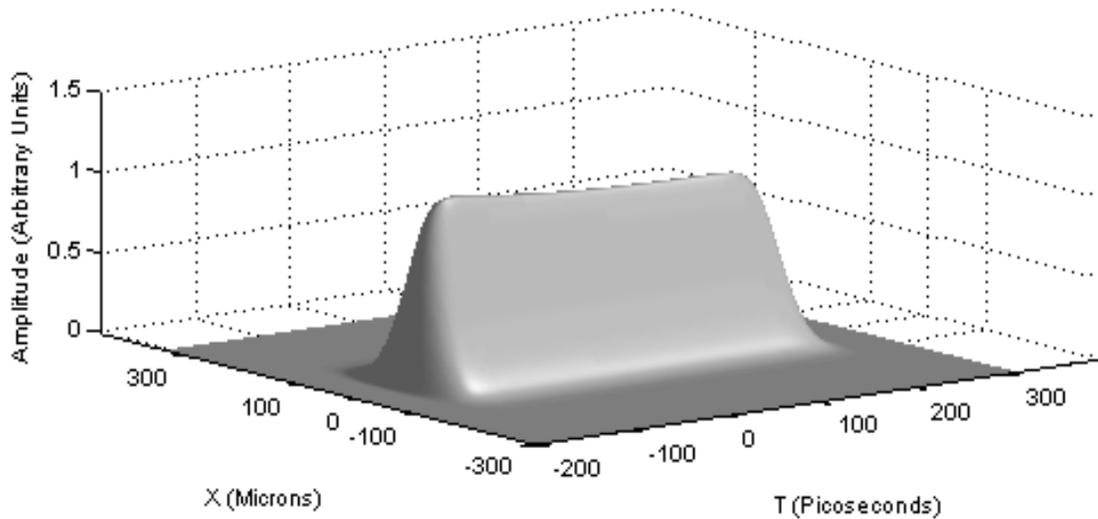
Figure 2.3. Three-dimensional pulse representation. Here, the *x* and *y* spatial dimensions define the pulse shape, while the temporal dimension displays the pulse duration. The pulse is now finite in time and is no longer a continuous beam.

An initial beam profile such as the one shown in Figure 2.1 is required for the 3D code to model pulse propagation correctly. For the finite pulse propagation model, inputting the desired parameters into the 2D code and initializing the program accomplish this. The key input parameters are the pulse waist size, initial pulse power or peak intensity, and desired grid size. The grid has a certain number of elements, defined as *nx*, while the total physical size of the grid is broken into discrete steps, defined as *dx*. The product of *nx* and *dx* returns the length scale of the grid in meters. Once these parameters are chosen, the code is initialized and the field is saved to a file. This file is then used as an input field in the 3D code to begin the propagation. The 3D code loads the input field and uses it as the initial beam profile in the propagation model.

Stability Issues

Physically, the effects of self-focusing must be balanced by the generation of plasma and other losses to allow filaments to propagate over long distances. In order to model this propagation, it is desired to find mathematically stable solutions emulating this physical balance. However, the solutions tend to be unstable because those with more or less than exactly one critical power will eventually collapse or diffract [19]. Any slight perturbation of the field causes the model to collapse or diffract the pulse. This is due to the unstable mathematical balance between self-focusing and diffraction of the beam solution [4]. In Chapter 4, the effects of initial beam powers that are several times the critical power on the propagation of a pulse will be examined.

While including the generation of plasma in these filament models would theoretically allow for a balance to be reached and therefore filament propagation to take place, short (less than one picosecond duration) UV pulses have previously been shown to be unstable due to the delayed response of the Kerr effect and plasma defocusing [26]. Schwarz and Diels assume in their model that the leading edge of a pulse can develop into the steady state middle region, or flat portion of the pulse [20]. These long pulses are based on Kerr and plasma defocusing response times that are instantaneous, which should supposedly avoid the instabilities that cause the breakup of short pulses. Niday looked at both spatial and temporal modulational instabilities in long pulses to determine their stability, and the effect these perturbations and transient edge effects would have on the propagation of the filaments [19].

As previously mentioned, the pulse can be modeled in two ways – as a CW beam or as a finite pulse. In each case, the pulse can be seeded with random noise, or

perturbations, before propagation begins. This noise is given as a temporal perturbation frequency, designated by Ω, or as a spatial perturbation field in the form of plane waves such as:

$$\begin{aligned} \varepsilon_+(x,y,z) &= u_+ \exp(\lambda z + i\vec{k}_\perp \cdot \vec{r}) \\ \varepsilon_-(x,y,z) &= u_- \exp(\lambda z - i\vec{k}_\perp \cdot \vec{r}) \end{aligned} \tag{2.17}$$

where $\vec{k}_\perp$ is a spatial frequency and transverse wave vector. The perturbations can be purely spatial with $\Omega = 0$, time-perturbed, or a combination of the two types of perturbations. In a real pulse, all frequencies in a temporal perturbation would be represented because the pulse would contain the full spectrum. Because the grids used to model the pulses are finite in size due to the numerical method used, the frequencies used to seed the pulse with noise must be bounded at some upper limit. In the current model, however, the method in which the noise frequencies are bounded prevent the model from propagating short pulses on the order of 100 fs or less. This is due to the pulses being at frequencies that are being cut out by the bounding methods. Therefore, it is not currently possible to model noise at the same time as short pulses less than 100 fs in duration due to this windowing conflict. This could be remedied in future work by changing how the unwanted frequencies are filtered in the model.

As mentioned above, Schwarz and Diels assume that the leading edge of a pulse should develop into the steady state region, which forms the flat, middle portion of the pulse [20]. The expression steady state refers to neglecting the time dependence of the plasma, and assuming that it does not change over the time scale of the pulses being modeled. This allows you to set $\frac{\partial \rho}{\partial t} = 0$ and solve directly for your plasma term. In

25

addition, this steady state solution must be stable. However, Niday determined that even when starting with a steady state solution and no edge effects, the leading edge undergoes a series of collapses that cause a collapse of the pulse as it evolves in time [19]. The combination of transient edge effects and the growth of temporal and spatial instabilities lead to the collapse of the pulse over a much shorter distance than is desired. In addition, Niday found that the pulses are unstable for all values of Ω and $k_\perp$ [19]. Chapter 3 concentrates on possible initial conditions or pulse characteristics that mitigate or stall the transient edge collapse events in long pulses. A study was also conducted to determine if the collapse events or pulse structure could be characterized to determine a pattern in the pulse collapse, possibly leading to a way to predict how far the pulse will propagate before it collapses, or in what manner the pulse will collapse based on initial conditions.

Optical Solitons

An optical soliton is a type of wave packet that can propagate over long distances without distorting. Like light filaments, solitons are created because the Kerr nonlinearities balance with dispersive effects that would defocus the pulse, such as group velocity dispersion [21]. Solitons have been useful in the telecommunications industry because of their ability to propagate over long distances in fiber-optic communication applications without changing their shape. The distortion-free propagation is possible due to the balance between self-phase modulation and group velocity dispersion, which preserves both the pulse shape as well as the pulse spectrum [21]. In the case of the long pulses being studied here, it has been shown that the pulse can break up into a series of much narrower pulses with even spacing between them [19]. If each of these collapse

elements could behave as a soliton, these smaller pulses would still be able to propagate long distances despite the longer pulse breaking up. However, solitons do not exhibit certain properties of light filaments such as the generation of a supercontinuum of light, and the mathematical expressions governing them can be solved analytically rather than numerically, as is the case with light filaments.

Because the focus of this study is on what occurs when a long UV pulse collapses on its leading edge as it propagates, the behavior of solitons is important because if the pulse collapsed into a series of soliton-like pulses, this would allow the energy of the initial long pulse to continue propagating even after it has collapsed, just in a different form. Rather than propagating as one long pulse, the energy would propagate as a train of many small, evenly spaced solitons. Therefore, a short pulse model also becomes important as the numerical methods used in the modeling program need to be capable of resolving and accurately modeling pulses much shorter than the initial pulses if the collapse events do exhibit soliton-like behavior. This behavior would effectively circumvent the collapse of the long pulse and still allow energy to be transferred over long distances, albeit in a different form.

The fundamental soliton or first-order soliton corresponds to the case of a single eigenvalue determined by solving the nonlinear Schrödinger equation given as

$$i\frac{\partial A}{\partial z} = \frac{\beta_2}{2}\frac{\partial^2 A}{\partial T^2} - \gamma|A|^2 A \qquad (2.18)$$

where A is the amplitude of the pulse envelope, T is the width of the pulse, β_2 is the group velocity dispersion parameter, and γ is the nonlinear self-phase modulation parameter [21]. A pulse is designated as a fundamental soliton because the shape of the pulse does

not change as it propagates [21]. By solving Equation 2.18, an expression for the fundamental soliton can be derived and is given by

$$u(\xi, \tau) = \operatorname{sech}(\tau)\exp(i\xi/2) \qquad (2.19)$$

where ξ is an eigenvalue resulting from solving Equation 2.18, and τ is a ratio of the pulse width to the initial pulse width [21]. The benefit of this solution is that it can be obtained directly from the nonlinear Schrödinger equation and is an analytic solution, rather than one that needs to be determined numerically. Another way in which solitons differ from the pulses used to create light filaments in the current numerical model can be seen in Equation 2.19, where the shape of the soliton is a hyperbolic secant function, rather than a Gaussian curve. This could have an effect on the ability of the current code to represent solitons accurately, as it uses a Gaussian to model the pulse shape. Additionally, the shape of the individual collapse events is not known, because they can not be fully resolved, so they too could not match the requirements of pulse shape and power to form a soliton.

If an initial pulse does not match the peak power of shape requirements to form a soliton, the pulse may evolve as it propagates to eventually form a soliton [21, 27]. The effect of the initial pulse shape can be studied numerically by solving the standard form of the nonlinear Schrödinger equation given by

$$i\frac{\partial u}{\partial \xi} + \frac{1}{2}\frac{\partial^2 u}{\partial \tau^2} + |u|^2 u = 0. \qquad (2.20)$$

Some energy may be shed in this evolution process, and the pulse may broaden or narrow to reach the desired shape required to form a soliton [21]. This could allow a Gaussian or

super-Gaussian pulse to evolve into a soliton by evolving into a pulse with a hyperbolic secant shape.

Summary

The propagation equation used to describe the behavior of the light filament can be numerically modeled in both two and three dimensions to study characteristics of pulse propagation. The split operator method is used to accomplish this propagation modeling. Specific factors in the propagation such as the critical power required to create a filament and issues regarding the stability of the pulse are of particular interest because of the effects they have in how the pulse behaves as it propagates. Finally, despite the propagation equation being simplified because of the relatively long pulses being investigated, short pulse behavior is also important due to the nature and size of the collapse events that occur on the leading edge of the pulse. The behavior of optical solitons is relevant because the collapse events may be able to continue propagation once the longer pulse has dissipated into a series of short peaks.

III. Methodology

Chapter Overview

      This chapter discusses the various methods that were used to attempt to understand the collapse that a pulse undergoes during propagation due to the transient properties of its leading edge. The methods can be separated into two parts: varying the numerical parameters of the model, and varying the physical parameters of the model. Numerical parameter variations include altering the spatial and temporal grid sizes used to model the pulse, and the size of the propagation step used while propagating the pulse. The physical parameters include the initial peak power used to generate the pulse, the plasma decay rate and including physical characteristics in the propagation equation such as group velocity dispersion.

Numerical Parameters

      The propagation model has many parameters that can affect the propagation of the pulse as well as the instabilities leading to the collapse of the pulse. It was first necessary to duplicate the results of Niday [19] to verify that the model was working correctly. Once correct operation of the code was established, runs with variations on these numerical parameters were conducted to determine what effect the parameters had on the propagation of the pulse. Figure 3.1 shows the field profile to which these varying numerical parameter runs were compared, which is a replication of results from Niday [19]. In addition, these numerical parameters had a direct relationship to the speed at which the code ran, so if fewer elements in the spatial grid or a larger step size could be used and return the same results, the model would complete more quickly and testing

would be more efficient. While straightforward, the grid characteristics were important because they were the only means of capturing the information of the field as it propagated. Because the collapse events tended to reduce to a size and spacing on the order of the grid size, efforts to capture as much information about these collapse peaks were important, and by varying the grid parameters it was hoped to be able to fully resolve the structure of the collapses.
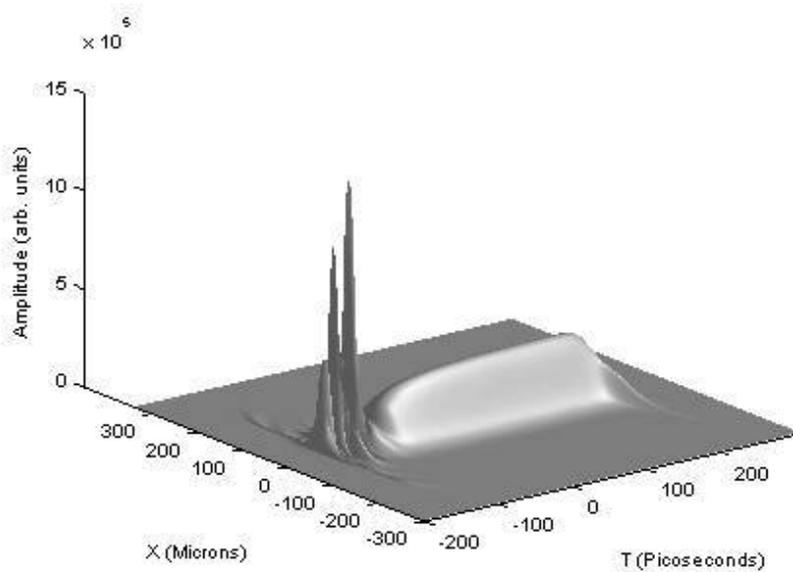
Figure 3.1. Finite pulse after 0.25 meters of propagation, with an initial peak power of 500 MW. This pulse profile duplicates results from Niday [19] and will be used as the basis of comparison for future runs using varying parameters to determine what effect the changes had. The parameters used in this run were 128 elements in the spatial dimension, 512 elements in the temporal dimension, and a $500 \mu m$ step size.

First, the grid size used to establish the spatial dimensions of the field was varied between 64 and 128 elements to determine what effect this had on the propagation of the pulse. For each case, a finite pulse with no losses and no noise was created and

propagated in propagation steps of 5×10^{-4} m in the 3D code. Apart from the grid size, the initial conditions were chosen to duplicate results from Niday [19].

The propagation step size was also varied. Because Niday used 5×10^{-4} m as his step size, this was modeled first, resulting in a duplication of his results when combined with a grid size of 128 elements [19]. Step sizes of 0.005 m and 0.05 m were then compared to these results. These step sizes were combined with grid sizes of 64 and 128 elements to determine what effects these parameters and their combinations had on the pulse propagation. It is important to note, however, that in the 3D model the size of the temporal grid remained at 512 elements with a time step of one picosecond throughout all of these variations. This was due to the duration of the pulse remaining constant at 400 ps to ensure that a long UV pulse model was captured fully in the temporal grid.

Finally, the time step size was adjusted in order to test for convergence of results. Because the peaks collapsed to dimensions that were comparable to the time grid spacing, the collapse events were not considered to be fully resolved and the finite grid was artificially limiting the collapse of the pulse. If the results converged as the time step was made smaller, then the peaks would not be able to be fully resolved. In these runs, the initial power was held constant at 500 MW and the propagation step size remained at 5×10^{-4} m with a 128 element spatial grid. The pulse was 10 ps in duration. Additional time convergence tests used a 10 ps duration, 250 MW pulse and the MPI coefficient β was increased by a factor of 10 to increase losses.

Physical Parameters

Once an optimal combination of grid, propagation and time step size was determined, physical initial conditions describing the type of initial pulse used to start the 3D propagation were examined. The desired outcome was a way to predict the collapse rate of the pulse based on the initial beam power that was used. Niday concluded that the collapse rate of the pulse was linear [19]. The question remained whether this linear rate would increase or decrease with initial peak power. By starting with varying peak powers in finite pulses with no noise seed or losses, the rate of collapse of the pulse could be measured as a function of the amount of the pulse that had been consumed at a given propagation distance. While the output from the code using OpenGL was sufficient to roughly estimate collapse rates, MATLAB plots were generated to more accurately predict the rates using on-axis 2D plots as shown in Figure 3.2. Here, a pulse of length 200 ps has traveled 0.25 meters along the z-axis. Because the collapse events have consumed 75 ps on the x-axis (time axis) of the plot, it can be concluded that the collapse is consuming the pulse at roughly 300 ps/meter of propagation. This collapse rate is simply the amount of pulse consumed in seconds divided by the propagation distance of the pulse in meters.
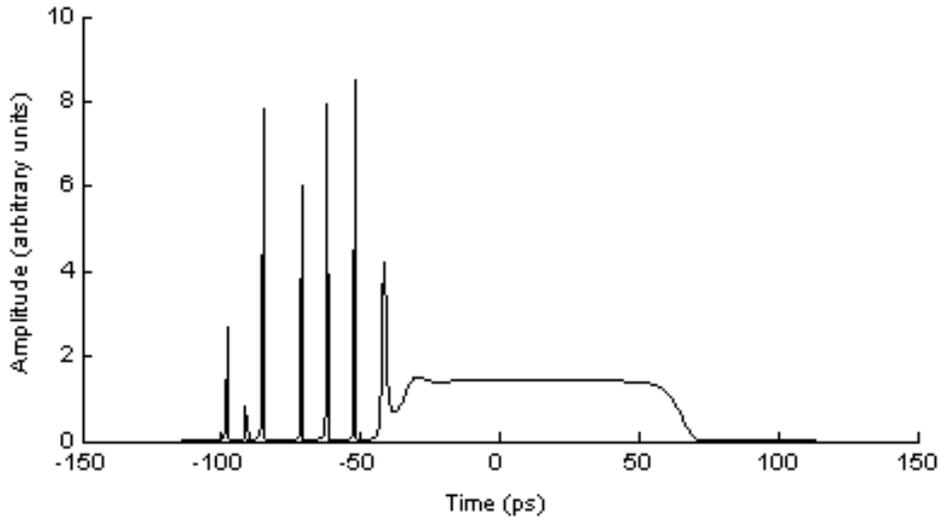
Figure 3.2. Two-dimensional representation of pulse collapse used to measure collapse rates. Here, the initial peak power was 500 MW and the pulse has propagated for 0.25 m. The pulse is being consumed at a rate of roughly 300 ps/m.

Starting with lower initial powers, the power was slowly increased for each run and the collapse rates compared at equal propagation distances. In a second series of runs, the initial conditions were held constant but loss effects were included in the propagation models. Again, the pulses were compared after a fixed propagation distance to determine what effect the initial power had on the collapse events.

Next, the electron-positive ion recombination rate was adjusted to determine if the absorption rates were connected to how the pulse collapsed. Because this term affected the amount of loss present in the model, varying the plasma absorption term effectively increased or decreased the loss that was controlling the pulse propagation by changing the rate of decay of the generated plasma. It also had an effect on the balance required for filament formation and propagation.

Group Velocity Dispersion

Group velocity dispersion causes a wave to spread into separate spectral components with different frequencies, due to the dependence of a wave's velocity on its frequency. This spreads the pulse out temporally in the same manner that diffraction spreads a pulse out spatially. In fact, the propagation equations for spatial and temporal propagation are very similar [24]. The propagation of a one-dimensional Gaussian beam is described as

$$\frac{\partial^2 \psi}{\partial y^2} - 2ik\frac{\partial \psi}{\partial z} = 0 \ , \tag{3.1}$$

while the group velocity dispersion propagation term is represented by

$$\frac{\partial^2 \mathcal{E}}{\partial t^2} - \frac{2i}{k^{"}}\frac{\partial \mathcal{E}}{\partial z} = 0 \ . \tag{3.2}$$

With some simple algebra, Equation 3.2 can be rearranged to match the GVD term in Equation 2.1. The GVD term in the original propagation equation was restored to the code as an additional linear operator in the form of

$$-\frac{ik^{"}}{2}\frac{\partial^2 \mathcal{E}}{\partial t^2} \ , \tag{3.3}$$

where $k^{"}$ is a normal GVD quantity equal to 200 fs^2 / cm in the UV range [19]. Because the long pulses being modeled are many picoseconds in duration, group velocity dispersion (GVD) can generally be neglected because of the relatively large time scale of the pulse length. However, in the case of short pulses of 100 femtoseconds (fs) or less in duration, GVD can play a role in the way the pulse behaves as it propagates. This is due to the relationship between the GVD parameter and dispersion length, given by

$$L_D = \frac{T_0^2}{|\beta_2|} \qquad\qquad (3.4)$$

where L_D is the dispersion length, T_0 is the pulse half-width, and β_2 is the GVD parameter [21]. The dispersion length controls the amount that the pulse broadens. Short pulses broaden more because their dispersion length is smaller.

Long pulses have been demonstrated to be unstable and collapse on the leading edge, causing them to break down into a series of smaller events. Because these collapse events are much shorter in length than the overall pulse, possibly on the order of femtoseconds in duration, GVD could determine how the pulse continues to propagate after it collapses by affecting the individual collapse peaks once they form, balancing the self-phase modulation of each peak to create solitons. Figure 3.3 illustrates a one-dimensional Gaussian pulse slowly dispersing temporally as it propagates along the *z*-axis due to the effects of GVD. Note that the broadening and flattening of the pulse is very similar to spatial diffraction, just over a much longer propagation distance.
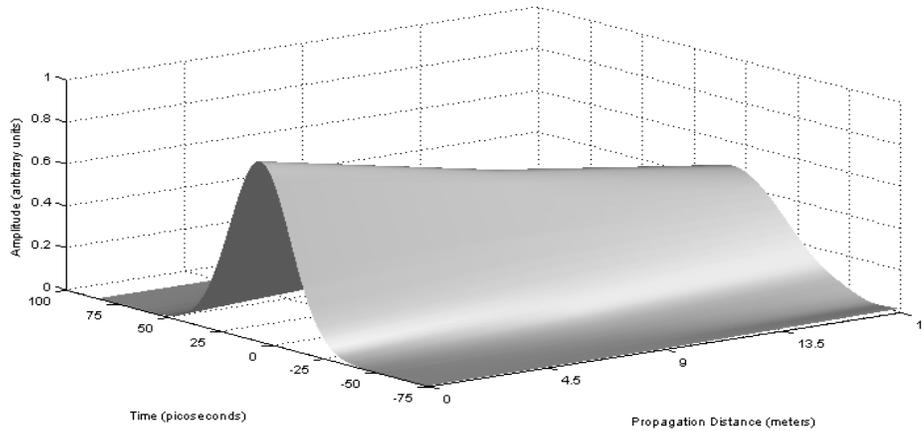
Figure 3.3. 100 fs 1D Gaussian pulse dispersing temporally as it propagates in the *z* direction. In this case, the pulse has propagated 45 meters. The effects of GVD are much more subtle than the normal spatial dispersion of a Gaussian beam. Each step along the *z* axis represents the distance that the 1D pulse has traveled, making this figure a history plot showing the evolution of the 1D Gaussian shape as a function of propagation distance.

In telecommunications and other applications involving solitons, GVD is undesirable because it interferes with the long distance propagation of the pulse and any information that it may be carrying [21]. To correct this problem, a technique known as chirping causes the different frequency components of a wave to leave at different times from the same origin [1, 21]. By chirping the wave initially, it is possible to alter the speed of the higher or lower frequency components so that they reach a certain point in phase and at the same time once the wave has propagated some distance. For example, in a negatively chirped pulse, the shorter, or blue wavelengths leave before the longer, or red wavelengths from the laser compressor [1, 21]. The negatively chirped pulse shortens temporally as it propagates, and once its intensity satisfies the conditions for filament formation, the supercontinuum is formed [1].

The ability to model short pulses is important for two reasons. First, very intense pulses have not been experimentally demonstrated for pulse durations of more than a few picoseconds in the UV range [6, 28]. A frequency doubled or tripled laser is required to reach the UV wavelengths used, and the level of power output required is generally not possible for such a long pulse. By shortening the duration of the pulse, experimental verification becomes possible.

The second reason that a short pulse model is desirable is that the collapse events are much shorter in duration than the overall pulse length. Initially, the long pulse runs were made without including GVD, because its effects could be neglected. However, as the time scale of the collapse events was studied, GVD was included in the code partly to see if this had any effect on the propagation of the pulse or its collapse events. Including

GVD was also important to determine if the code was able to accurately model short pulses on the scale of less than 100 fs. Therefore, if the code was able to accurately model pulses a few femtoseconds in duration, the short collapse events could be observed continuing to propagate, or several very short pulses could be looked at separately from the long pulse. With the addition of GVD to the code, and appropriate time step sizes, pulses of 100 fs or less were modeled to see if they exhibited any sort of soliton-like qualities as they collapsed.

Summary

Finite pulses that had not been initially seeded with noise frequencies were examined to study their behavior under a variety of conditions. The size of the propagation step and spatial grid were varied to determine what effects, if any, these numerical parameters had on the pulse and its eventual collapse. The temporal grid was studied to test for convergence of results and full resolution of the collapse events. Physical initial conditions, such as initial peak power, electron-positive ion recombination rate, and group velocity dispersion were also considered in an attempt to understand the source and behavior of the collapse on the leading edge of the pulse. Initial conditions such as the initial power used to create the pulse were varied to study the effect of these conditions on the rate of collapse of the pulse. Finally, the ability to model short pulses less than 100 fs in duration was added to the model to further investigate individual collapse events and the effect of GVD on individual pulses.

IV. Analysis and Results

Chapter Overview

This chapter covers the results of the various experimental runs outlined in Chapter 3. The effects of varying numerical parameters to determine the optimum setup for the model are discussed. Also, the effects of varying initial pulse power to determine the collapse rates of the pulses are shown. As an extension of varying the initial pulse power, the effect of peak power on plasma generation and the structure of the collapse events were investigated more closely. Finally, the inclusion of GVD in the model is covered and the results of the short pulse experiments discussed.

Results of Varying Numerical Parameters in Propagation Model

The results in Niday [19] were created with a spatial grid size of 128x128 elements and a temporal grid size of 512 elements. The first parameter to be tested was the spatial grid size. With each individual grid element representing 8 microns, the number of elements was decreased to 64 elements in both the x and y directions. The result of this grid variance was an inability to duplicate previous runs using a grid size of 128 elements. The collapse events seemed to take place at roughly the same propagation distance and evolved in the same manner at first. A comparison may be seen in Figure 4.1. However, as the collapse of the pulse grew more pronounced, the sides of the pulse appeared to go off the edge of the grid, which impeded the collapse of the leading edge from consuming the entire pulse. The smaller grid size led to an artificial increase in the pulse propagation length solely because elements of the pulse were going off the grid and

39

no longer contributing to the pulse collapse. Therefore, it was concluded that the grid size needed to be at least 128 elements in both spatial directions to get an accurate representation of pulse propagation, though a 64 element grid could be used for initial approximation runs to evaluate significant changes made to the code to save calculation time. This result illustrated the importance of capturing as much information as possible in the propagation of the pulse by increasing resolution in the grid used to define the field.

The propagation step size was also altered to determine how the propagation and collapse of the pulse were affected. For a step size of 5×10^{-3} m, the results closely mirrored runs using a step size of 5×10^{-4} m, though the collapse events on the leading edge were not quite as defined. Reducing the propagation step size to 5×10^{-5} m did not change the results, so convergence had been reached. Increasing the step size to order of magnitude to 5×10^{-2} m did not allow the model to sufficiently resolve the collapse events, and artificially increased the propagation length of the pulse. Again, to capture as much information about the pulse as it propagated as possible, a smaller propagation step size was required. However, because the results did not vary for step sizes smaller than 5×10^{-4} m, the step size did not need to be reduced further. The numerical parameters chosen by Niday [19] were confirmed to be the best combination of computational efficiency and resolution of pulse characteristics. The results of varying the propagation step size can be seen in Figure 4.2.

(a)
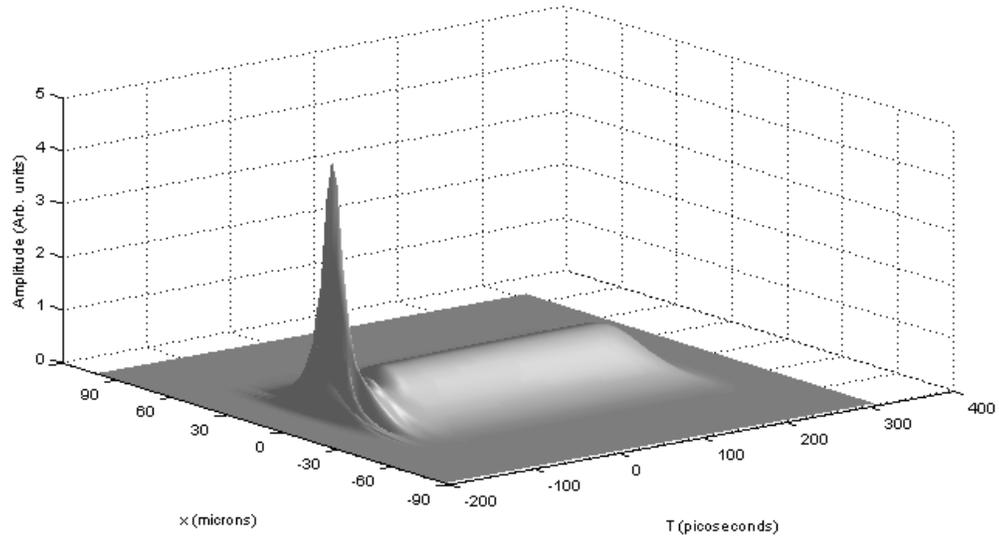
(b)
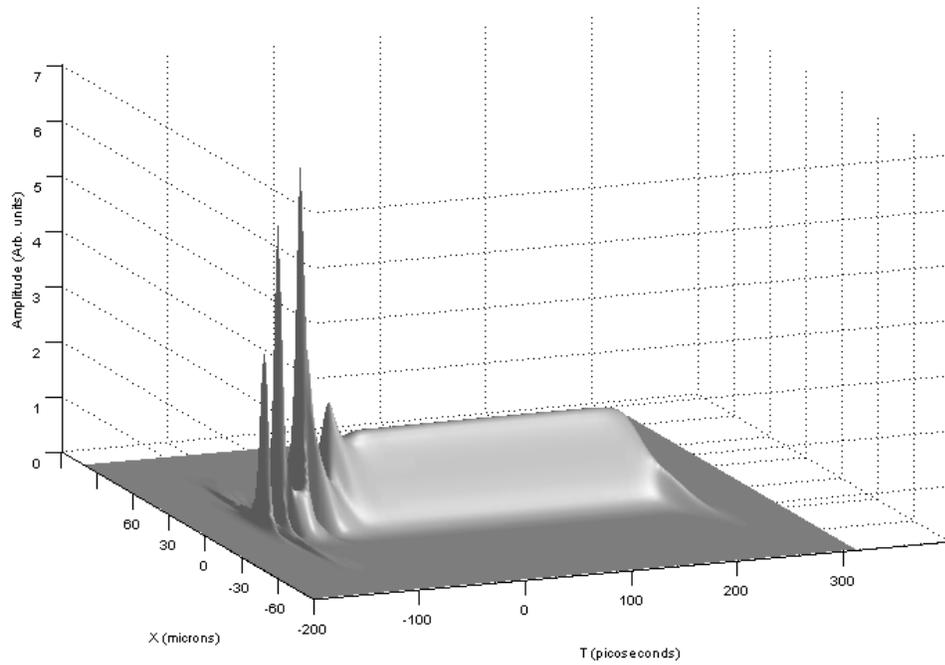
Figure 4.1. Results of a (a) 500 MW pulse propagated 25 cm using a 64 element grid to a (b) 128 element grid. Note that the pulse collapse is less evolved when compared to the 128 element grid, illustrating the lack of resolution available when using a smaller grid.

(a)
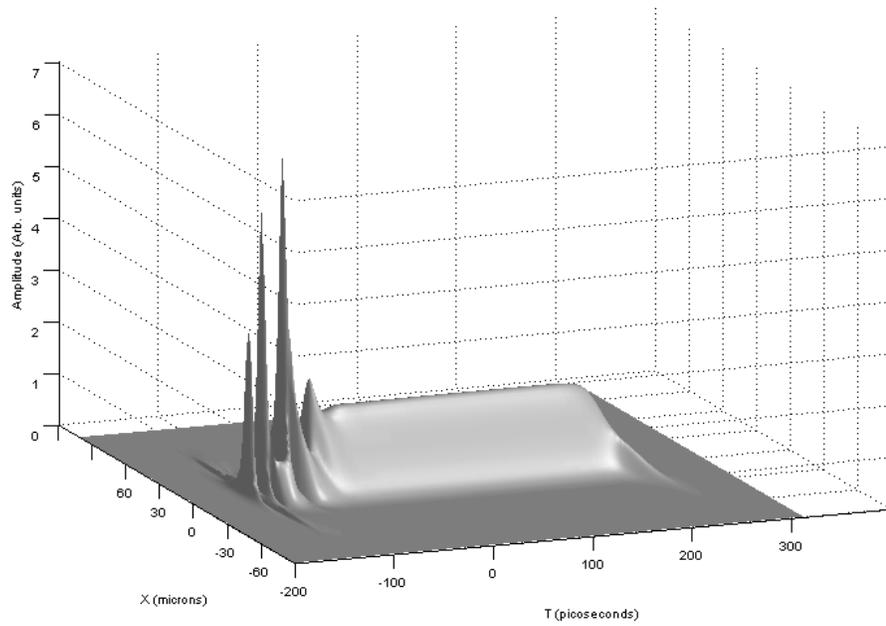
(b)
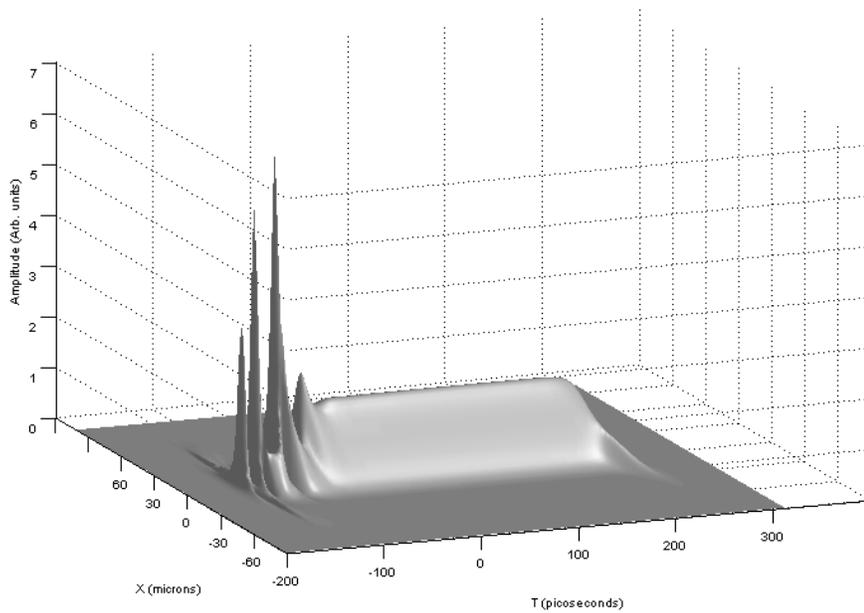
Figure 4.2. Comparison of 5×10^{-3} (a) vs. 5×10^{-4} (b) propagation step size. The finer step size results in slightly more defined collapse events though the differences are not obvious, so it was used in all future runs.

The time step size Δt was altered to determine if the results of the pulse collapse converged at a certain value. Once the first collapse event appeared on the leading edge of the pulse, the rest of the pulse evolution could be considered physically invalid due to the pulse exhibiting collapses of durations on the order of the grid spacing, or one time step size. As the pulse collapses, the collapse is being constrained by the grid size of the model which directly affects the physical validity of the results, rather than physical processes dictating what the model shows. An example of this problem is grid overflow in frequency space, which is covered in more depth in the section on trailing edge pulse collapse. This overflow causes numerical errors or artifacts to develop in the model and allows non-physical results to affect pulse propagation. Showing convergence of results in the time domain would strengthen the argument that the results the model returns are not invalid, but rather that conditions used to model the pulses need to be adjusted in order to give more realistic results and remedy the issue of the model interfering with the physical processes controlling pulse propagation. By demonstrating convergence of results in the time domain, strength is given to the argument that the model is no longer constraining the collapse of the pulse and conclusions may be drawn from the output of the model in various tests.

Figure 4.3 shows the initial results of decreasing the time step size for a 10 ps duration pulse to check for convergence. The collapsed peaks were generally very sharp and only had one grid element underneath the peak, so that nothing could be discerned regarding their shape or structure. Because the time step was directly related to the overall pulse duration, the specific step sizes used in the study could only be used in cases where a 10 ps duration pulse would be propagated with the model. Moving to

shorter duration pulses such as 10 or 100 fs would require smaller step sizes to be used to keep the full pulse profile on the grid used to model the pulse with an acceptable amount of resolution. Likewise, a longer duration pulse would require a larger step size for the pulse to fit onto the temporal grid. Therefore, it was more practical to consider a ratio of temporal step size to pulse duration. If the ratio between step size and pulse duration met the criteria, then the model was deemed to be resolving the pulse as accurately as it could while still using a reasonably sized time grid. The ratio determined to work the best was for the time step size to be $1/100^{th}$ of the pulse duration if using a supergaussian pulse profile, and $1/20^{th}$ of the pulse duration when using a Gaussian pulse profile. The ratio was defined as the total pulse duration as set by the initial conditions divided into the time step, Δt, which was also defined in the initial conditions used to create the pulse. This created a time grid that was manageable in terms of computing time but captured as much detail of the pulse as it propagated as possible.

No convergence could be seen when varying the time step initially, though the results were very close as the time step size was decreased. In all cases, reducing the size of the time step actually increased and narrowed the collapse peaks, which pushed the model further away from discerning any type of shape for each peak. Therefore, the temporal grid remained at 512 elements and the ratios determined above were used to model the pulse duration depending on the shape of the pulse used initially. These parameters were kept consistent when producing the results of the other studies investigated.

(a)
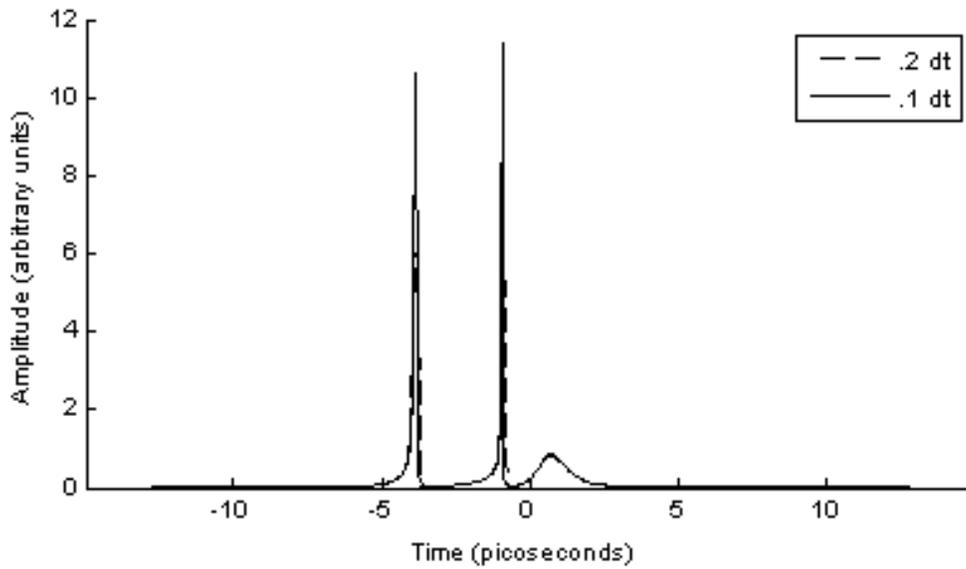
(b)
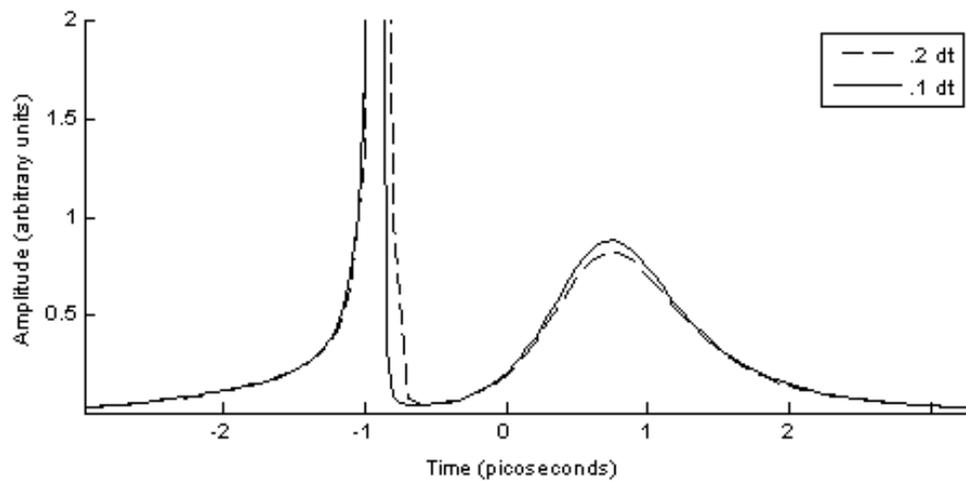
Figure 4.3. Time step convergence plots of the collapse of a 500 MW, 10 ps pulse after .25 m of propagation for two different values of Δt. Plot (b) represents a zoomed in area of (a), and the scaling of the plot has cut off the top of the first peak.

Because some of the loss terms associated with the plasma generation and other physical effects are not well understood, and may vary by an order of magnitude or more depending on the reference they are taken from [19], the MPI coefficient β was increased by a factor of 10 to determine what effect this had on the collapse of the pulse and convergence of results. This decreased the intensity of the collapse peaks created on the leading edge of the pulse because the loss was better able to control the rapid growth in intensity. The pulse power was also reduced from 500 to 250 MW. The combination of a lower pulse power and increased loss allowed a careful study of the leading edge of the pulse and the collapse that it underwent. The collapse events that were generated were examined and the results for runs made with steadily decreasing time steps were compared to check for convergence. The pulse used was 10 ps in duration with 250 MW initial peak power, and the time step was varied from 0.1 ps to 0.025 ps to check for convergence. The results can be seen in Figure 4.4. Making these changes led to the pulses converging as the time step was reduced.

Based on the variations in grid and propagation step size that were studied, it was determined that a 128x128 element spatial grid, a time step size according to the ratio determined above, and step size of 5×10^{-4} m were optimal for showing convergence of results in the pulse propagation and allowing the code to complete a specified number of propagation steps in a reasonable amount of time. In addition, the MPI coefficient needed to be increased by a factor of 10 to allow this convergence to occur. The parameters other than the new MPI coefficient value were used for all future runs of the model, so all of these results need to be revisited to determine what effect the new MPI value has on how the pulse propagates.

(a)
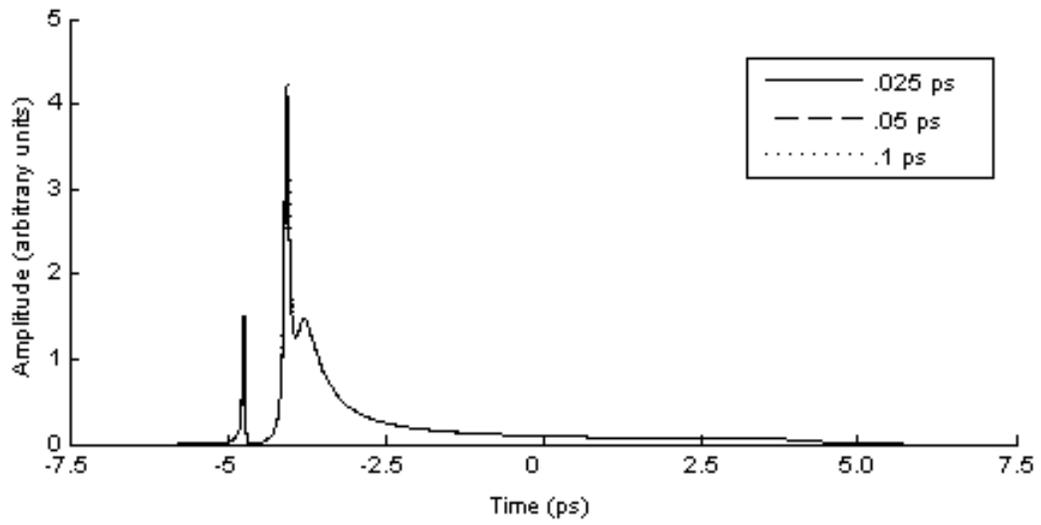
(b)
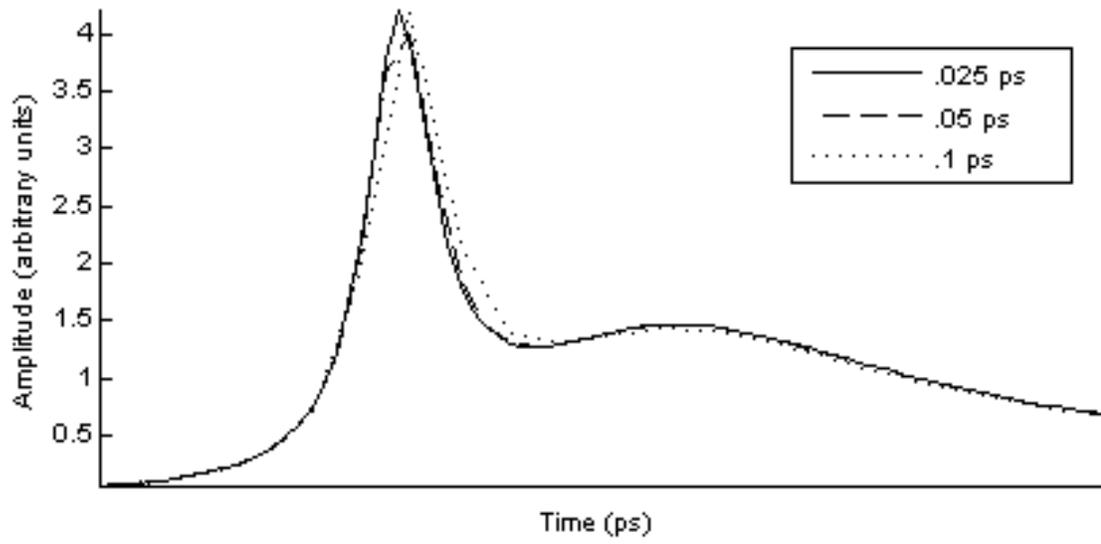
(c)
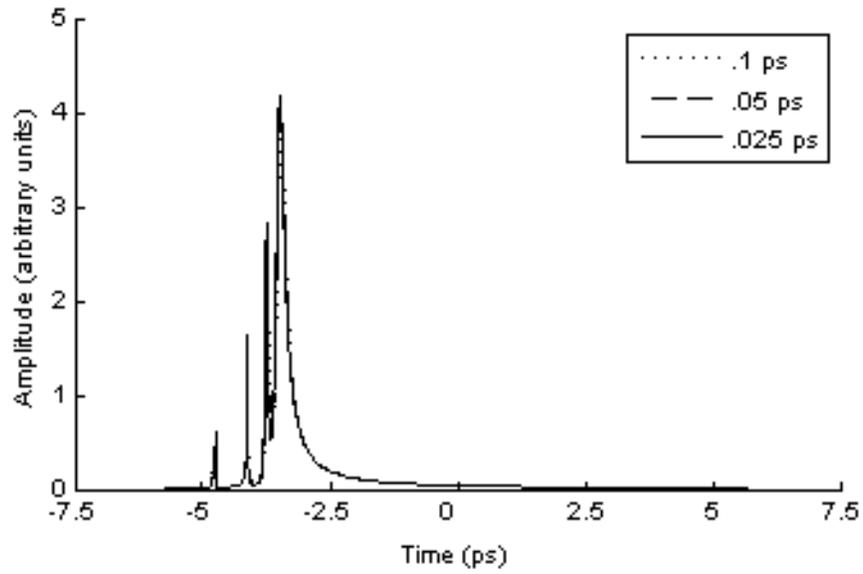
(d)
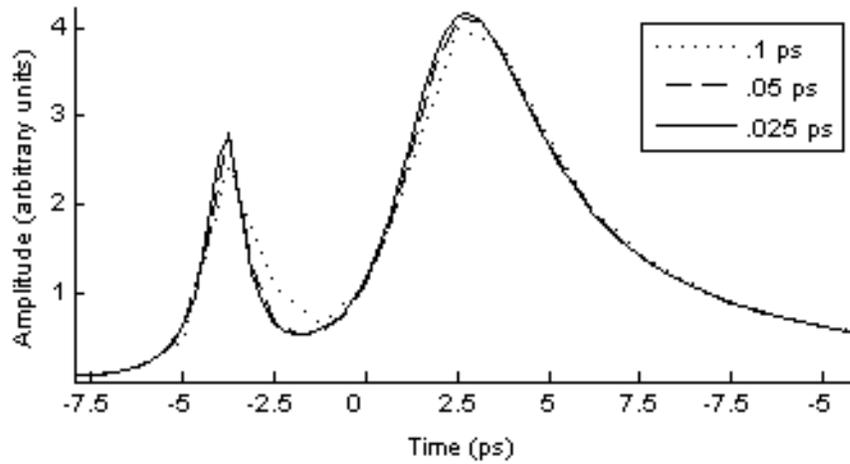
Figure 4.4. Plots showing the convergence of a 250 MW, 10 ps duration pulse using varying time steps to model pulse propagation. The plots show (a) the pulse after propagating 55 cm, (b) a close up view of the collapses at 55cm, (c) the pulse after propagating 1 m, and (d) a close up of the collapses at 1 m.

This convergence study resulted in a temporal grid size of 512 elements to achieve maximum resolution while allowing the code to complete each run within a reasonable amount of time, which was generally 6-8 hours for 0.50 m of propagation distance. However, the results of the additional time convergence studies point to adjustments that need to be made within the physical parameters used to model these pulses, including the MPI coefficient β, and future work is required to apply these changes to the other studies conducted using this model and determine what impact these adjusted parameters have on the results presented here.

Dependence of Collapse Rates on Initial Beam Power

When the numerical parameters of the model were initially tested, the hypothesis was that a higher initial pulse power would cause a linear, yet more rapid collapse of the pulse. This expectation was a result of initial tests that showed an increase in the number of collapse peaks generated with an increase in initial peak power. Using the numerical parameters determined in the previous section, tests were run in an attempt to extract an expression for the rate of collapse of the pulse as it propagated. The desired outcome was to use this expression to predict the distance a pulse could travel without collapsing, or to predict the rate at which a pulse would collapse based on its initial power. Figures 4.5 and 4.6 illustrate the result of these runs. The initial runs were made with no losses due to plasma or linear effects included in the model. Later runs included these losses to see if they mitigated the collapses. Inclusion of the losses did not eliminate the collapse events, though it did damp them slightly. While losses did reduce the intensity of the collapse peaks somewhat, they had no effect on the rate of collapse of the pulses due to the peaks

forming on the leading and trailing edges of the pulse. The collapse would occur regardless of whether losses were present in the model.
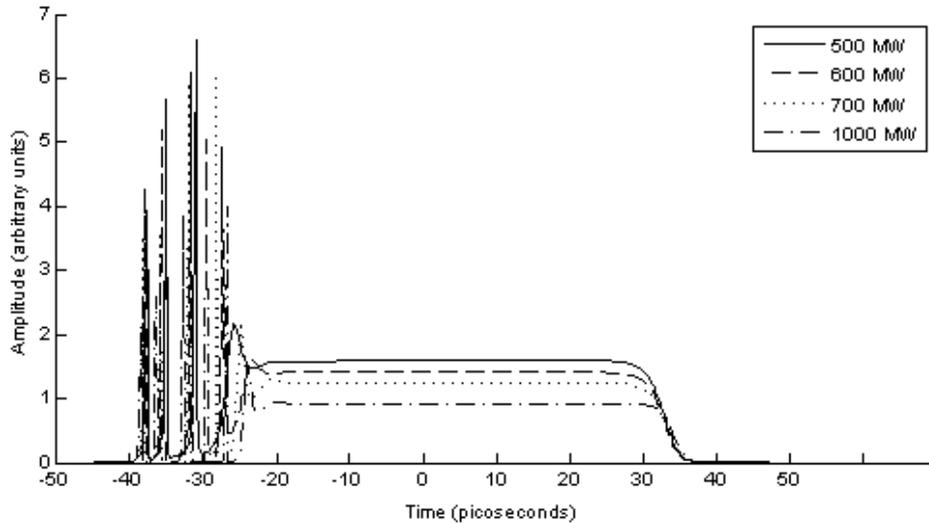
Figure 4.5. Increasing initial peak powers have little effect on the rate that a pulse collapses. After 0.50 meters of propagation, each pulse has collapsed roughly the same amount. However, note that the number of collapse events increases with peak power.

Increasing the initial power did not cause the pulse to collapse any more rapidly. Niday had previously determined that the pulse would collapse at a linear rate [19], but it became apparent that this rate was not affected by input power. The pulse would always collapse the same amount after a given distance of propagation. However, the number of collapse events did increase with initial power. For a higher initial peak power, collapse events would grow more rapidly and seed the next collapse on the leading edge of the pulse sooner, allowing more events to occur in a shorter distance of propagation. Lower powers would still collapse at the same overall rate by pushing the top of the pulse higher in intensity over a greater amount of the pulse, but it would take longer for the collapses

50

to fully form into sharp peaks and the collapse events tended to be smoother as the pulse

propagated.
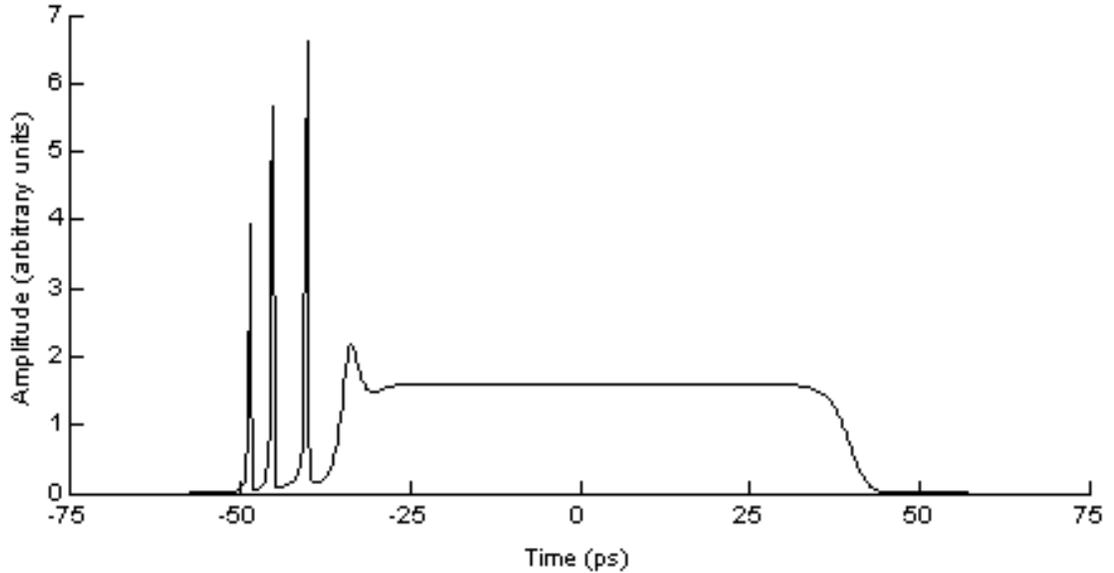
Figure 4.6. Field profile for a 500 MW field after 0.25 meters of propagation. The collapse event growing out of the leading edge of the pulse is wider (along the time axis) and is effecting a larger portion of the pulse than the collapse event in Figure 4.6.
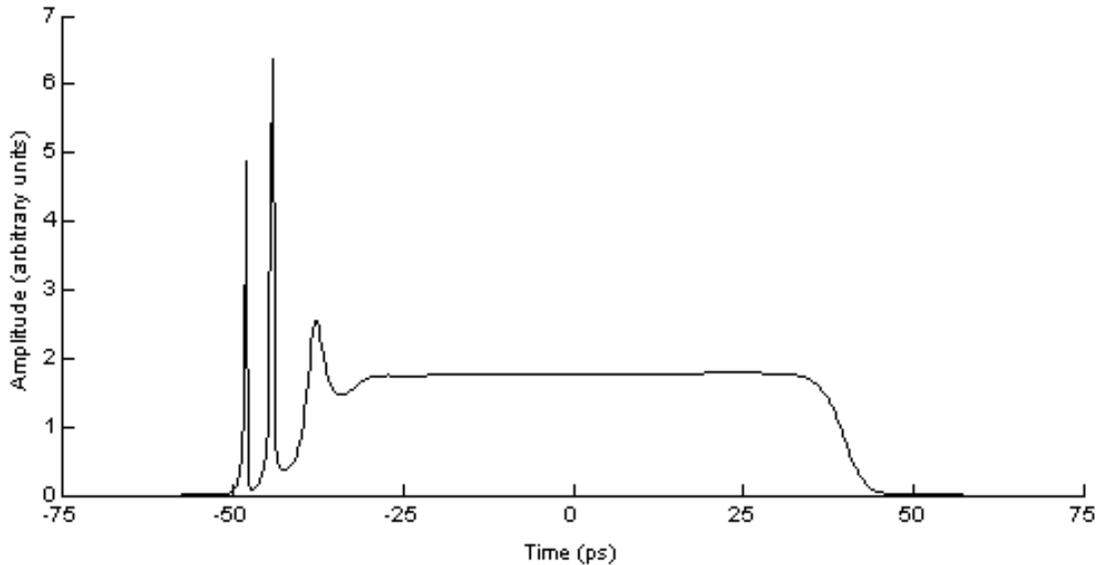

Figure 4.7. Field profile for a 1000 MW field after 0.25 meters of propagation. Note that there are more resolved collapse events after the same propagation distance than in the case of 500 MW. The total collapse distances are the same.

51

Relationship of Plasma Generation to Collapse Structures

The increased number of collapse events and their spacing can be attributed to the generation of plasma during the focusing of the pulse and its decay rate. A pulse with higher initial power will ionize the air sooner, resulting in more rapid plasma generation. Once the plasma reaches a certain intensity, it starts to defocus the pulse and the pulse intensity drops, which is consistent with the self-guiding theory describing the propagation of filaments. After the pulse intensity has fallen to a point where it is no longer able to maintain the plasma, the pulse can grow in intensity once more. This increase in intensity is once again caused by the self-focusing effects that are generated by the main body of the pulse. In a balanced, propagating pulse with no collapse events, this process would allow the defocusing effects to balance the nonlinear refractive index and long distance propagation could be possible. However, in the case where the leading edge of the pulse collapses into very intense, sharp peaks, the plasma is generated extremely rapidly and at very high levels. The drop in the intensity of the front edge of the pulse due to the plasma is almost immediate, and the collapse event becomes separated from the body of the pulse. Once the plasma has dropped back down to a lower intensity, the process repeats again. This violent cycle is caused by the manner in which the leading edge of the pulse collapses into a series of very intense spikes. Pulses with a higher initial power are more able to rapidly generate collapse events so the number of collapses increases with initial peak power. Figure 4.8 shows an example comparing a 400 MW power to a 1000 MW power to illustrate the fact that higher initial powers lead to more peaks being generated.

(a)
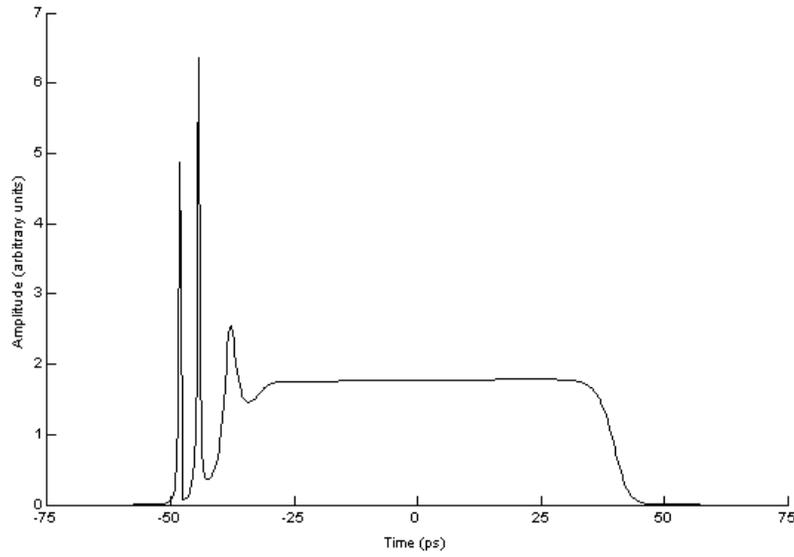
(b)
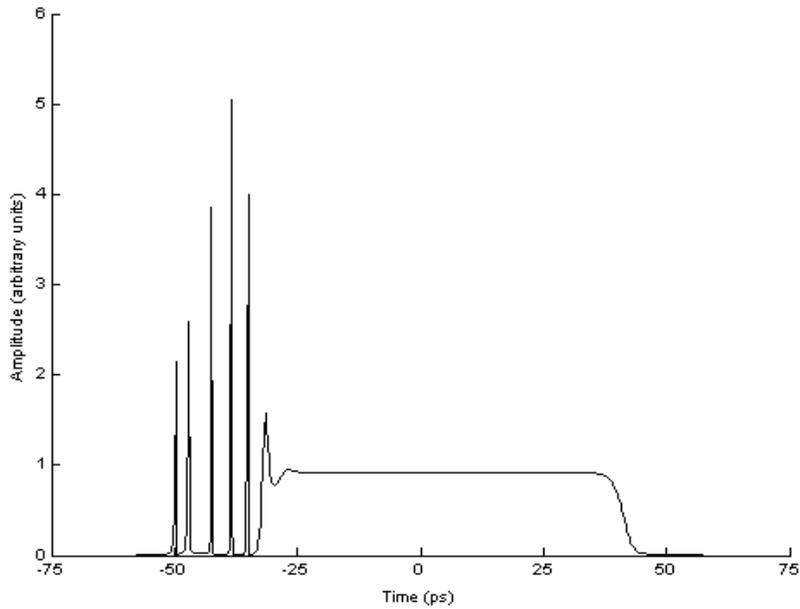
Figure 4.8. Comparison of 400 MW to 1000 MW pulse after 0.25 meters of propagation showing how lower powers lead to longer (measured as a fraction of total pulse duration), less distinguished collapse events. Higher initial powers result in more resolved collapses. In (a), while the next collapse event has been seeded it is very hard to identify from the main body of the pulse, so the collapse rate of (b) looks slightly higher. The actual collapse rates are the same.

53

The rate at which the plasma decays is not immediate, as there is a time scale associated with how long it takes the plasma to fall below the amount required to allow the pulse to intensify again. Figures 4.9 and 4.10 show the plasma intensity superimposed on the pulse intensity to illustrate the relationship between the two. It is evident that as the plasma decays down, the pulse begins to experience another collapse event on its leading edge and the process begins over again. The spacing between collapse events can be directly attributed to the rate at which the plasma decays after the intensity of the pulse falls off and is no longer able to support such a high intensity of plasma. Again, a higher initial beam power leads to a higher intensity, seeding the collapse events more rapidly, but also generating plasma at a greater rate. Therefore, even though there is no difference in the overall rate of consumption of the pulses due to initial beam power, the power does influence the rate and amount of plasma generated and leads to an increased number of collapse events on the leading edge of the pulse. The plasma, in turn, dictates the spacing of the collapse events.

The trailing edge of the long pulses also exhibited collapse events, though in a different manner than those on the leading edge. Instead of the leading edge continuing to collapse until the entire pulse was consumed, the trailing edge also began to collapse and the entire pulse broke down rapidly. The trailing edge only collapsed after the leading edge had consumed a significant amount of the pulse, and then the peaks grew rapidly. In addition, numerical errors due to the modulational instability of the pulse began to grow on the remaining flat portion of the pulse, and this noise grew exponentially, furthering the breakdown of the model's ability to accurately model the pulse.
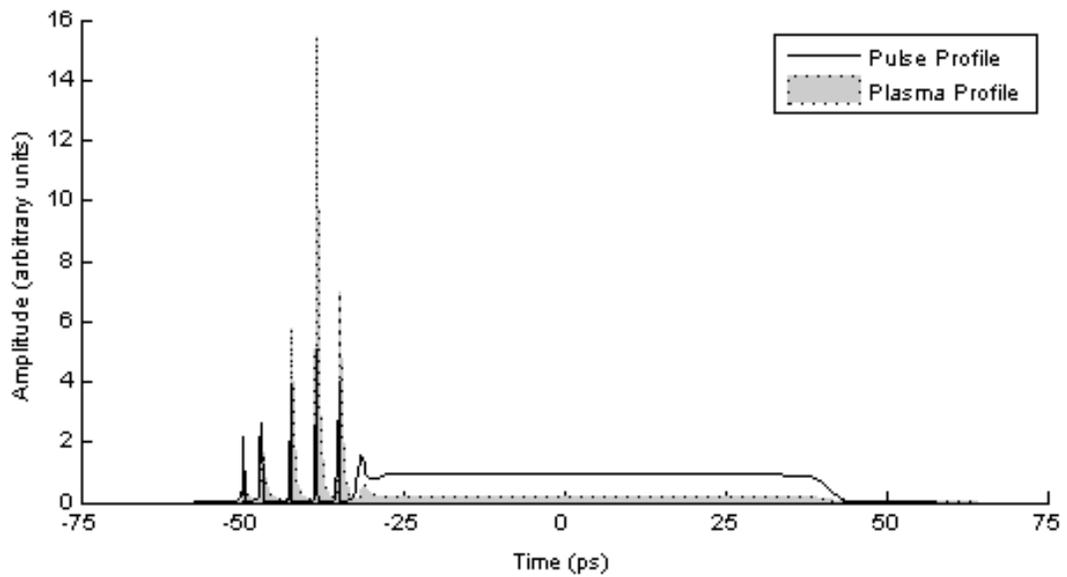
Figure 4.9. Comparison of time scale of collapse events with the plasma level for a pulse with 1000 MW initial peak power. The plasma level (solid plot) decays after the pulse intensity (line plot) drops down. Once the plasma has decayed, the next collapse event becomes evident. The plasma level has been normalized to allow comparison on the same scale as the pulse intensity.
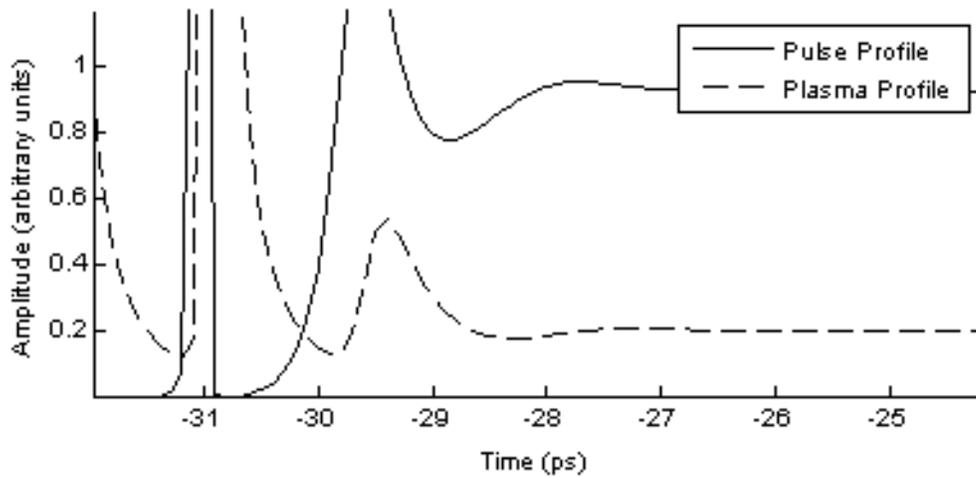
Figure 4.10. Close up view of the plasma level versus pulse intensity. Here it is more obvious how the plasma decays down to a lower level and allows the pulse to intensify once more in a new collapse event. Again, this figure is illustrating a zoomed-in portion of Figure 4.9, so several peaks have been cut off due to the new scaling.

55

Figure 4.11 depicts a 1000 MW pulse after it has propagated for 0.50 m. The collapse peaks on both edges and the numerical errors have caused the pulse to break down. The plasma intensity plot has been overlaid on the pulse profile so that the plasma generation can be compared to the collapse events taking place on the edges of the pulse.

Initial analysis showed that the plasma level on the trailing edge of the pulse behaved in the same manner as on the leading edge of the pulse. The collapse peaks forming on the trailing edge were separated by the plasma decay rate and their amplitude was also controlled by the presence of the plasma, though the intensities were lower than those on the leading edge of the pulse. In addition, the formation of the collapses was much more rapid than the collapses on the leading edge. The trailing edge collapses did not form and break off of the main pulse body one at a time. Instead, they grew concurrently out of the pulse. As both edges of the pulse collapsed, small peaks started to grow in the uncollapsed portion of the pulse due to modulational instability, and the model was no longer modeling the pulse shortly thereafter.

(a)
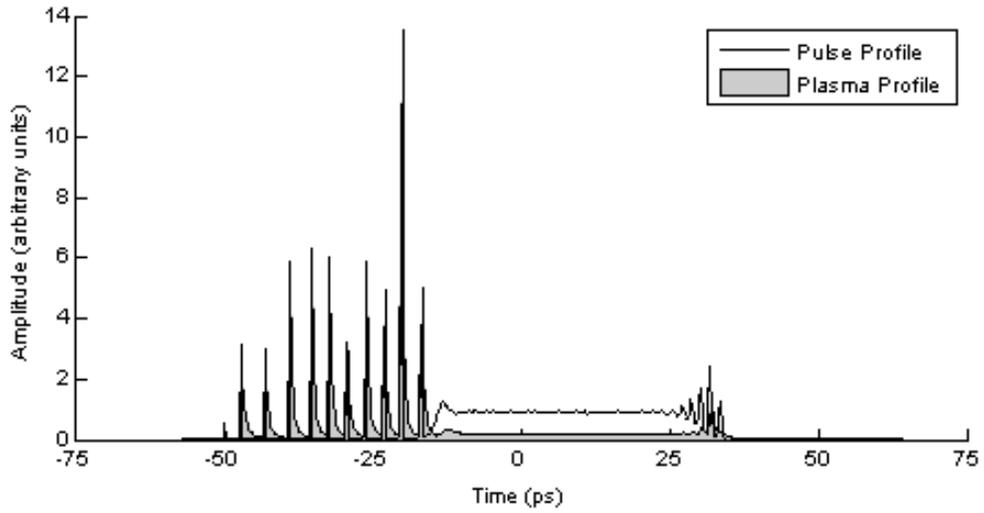
(b)
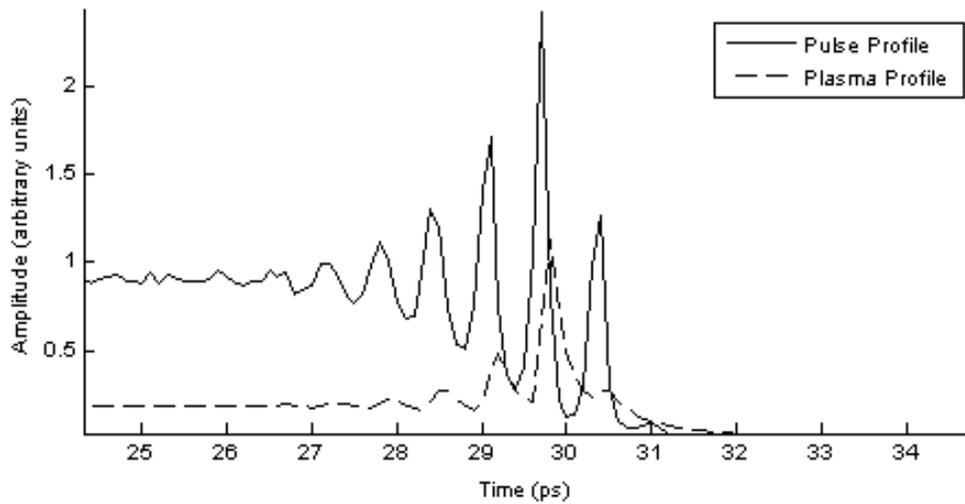
Figure 4.11. The collapse of the trailing edge of the 1000 MW pulse can be seen in (a). As previously shown in Figure 4.10, the plasma generation and decay rates dictate the spacing of the collapse peaks. Similarly, the peaks on the trailing edge of the pulse generate plasma in the same manner. Note the effects of modulational instability beginning to emerge from the flat portion of the pulse to the left of the trailing edge.

57

(a)
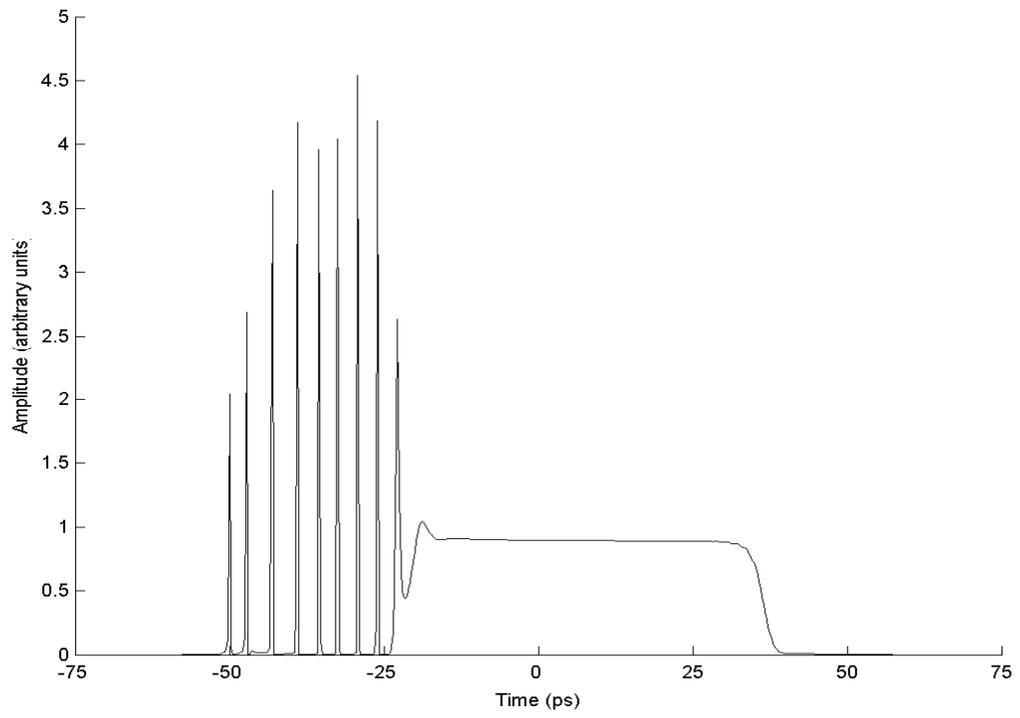
(b)
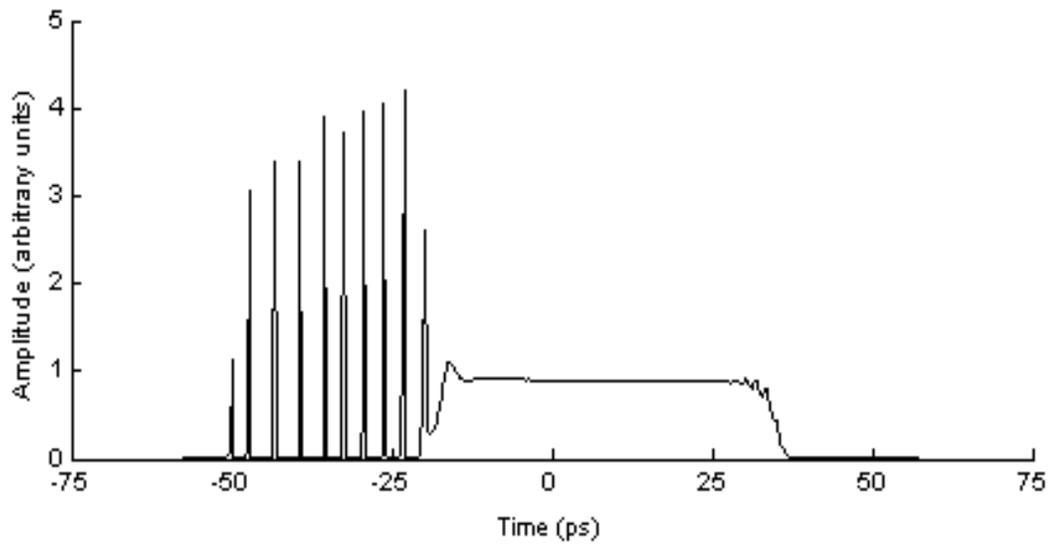
(c)
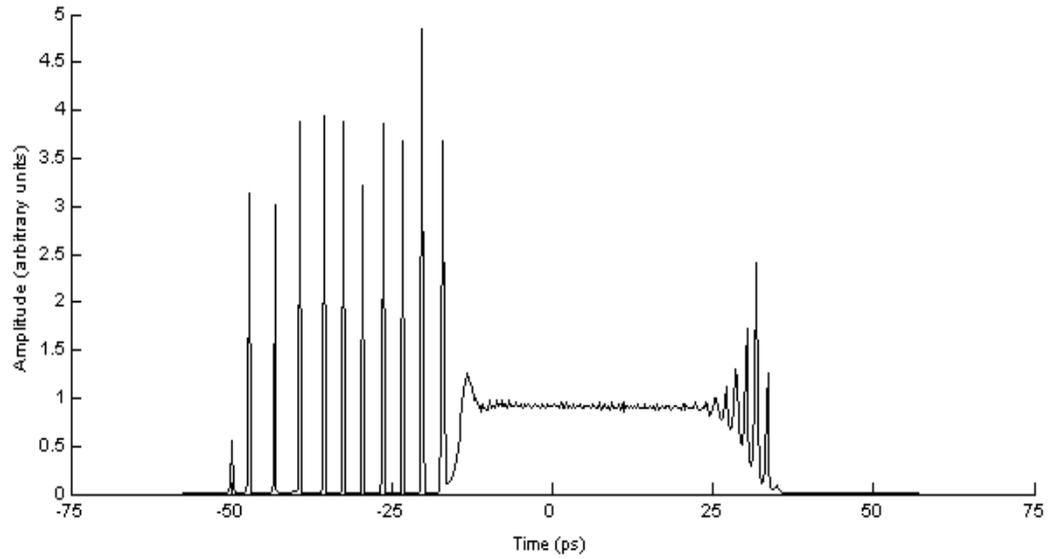
(d)
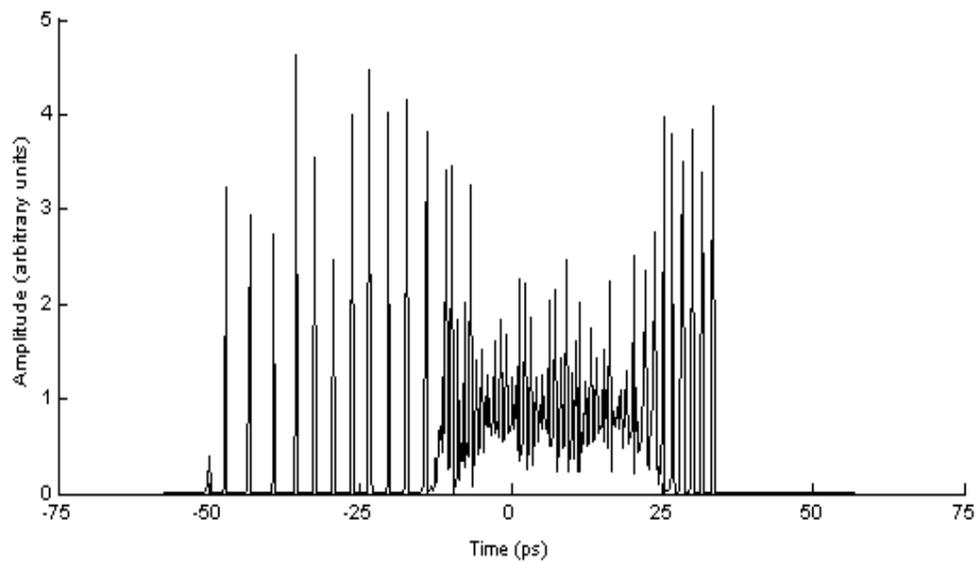
Figure 4.12. Collapse of 1000 MW pulse due to the leading and trailing edge effects. Note that once the trailing edge collapse peaks become prominent, failure of the code to model the pulse quickly follows. Also, the collapse events on the trailing edge grew at the same time, instead of one peak at a time like on the leading edge. The peak is shown at propagation distances of (a) 40 cm, (b) 45 cm, (c) 50 cm, and (d) 55 cm.

Another characteristic of the collapsing trailing edge was the way in which the edge of the pulse would begin to exhibit instabilities more rapidly as the initial power of the pulse increased. The distance that a pulse could propagate before the collapses on both ends of the pulse created instabilities that annihilated the pulse decreased as the power increased. This was not because of the rate of collapse increasing, but rather because the model was breaking down more rapidly once the collapse events on the trailing edge became evident. The earlier appearance of the trailing edge collapse was due to the greater intensity of the initial pulse, which allowed larger collapse events to occur on both edges as the pulse propagated. A pulse with lower initial peak power would propagate farther before the model no longer became valid (i.e., the pulse had completely collapsed into a series of smaller collapse events). Figure 4.13 illustrates the collapse of the pulse.

(a)

b)

61
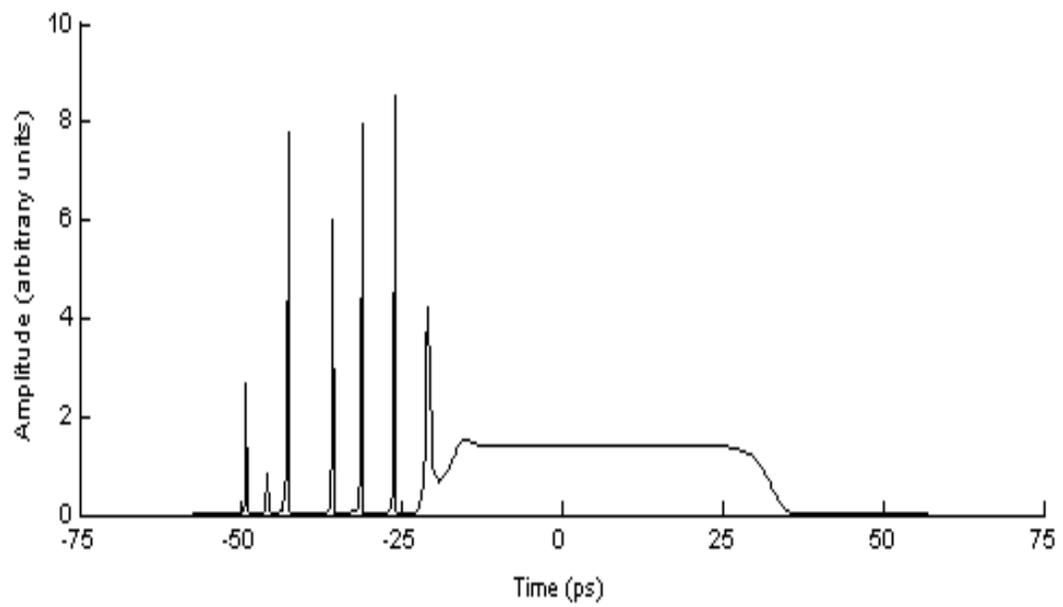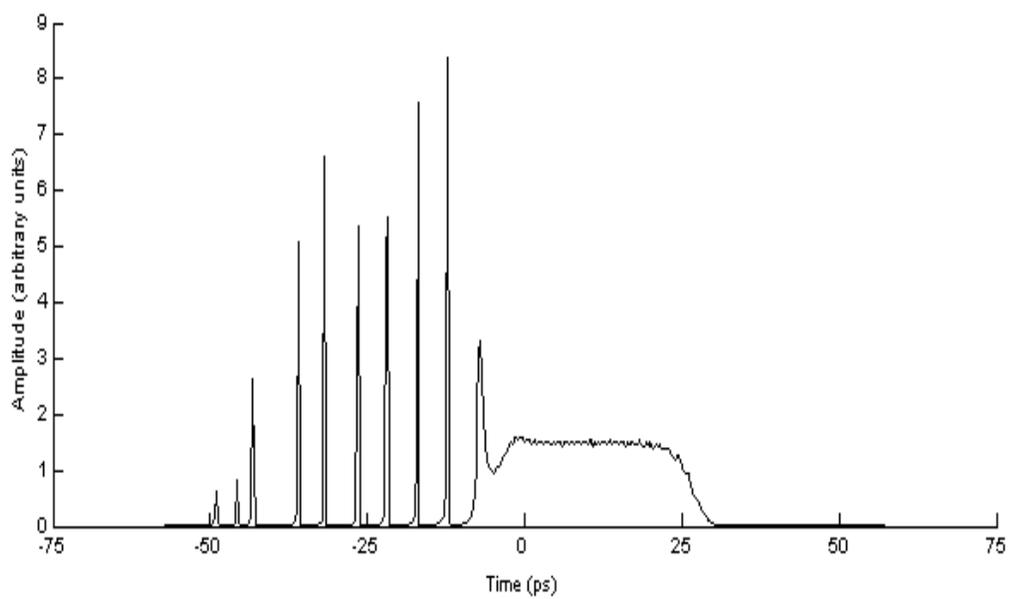
(c)
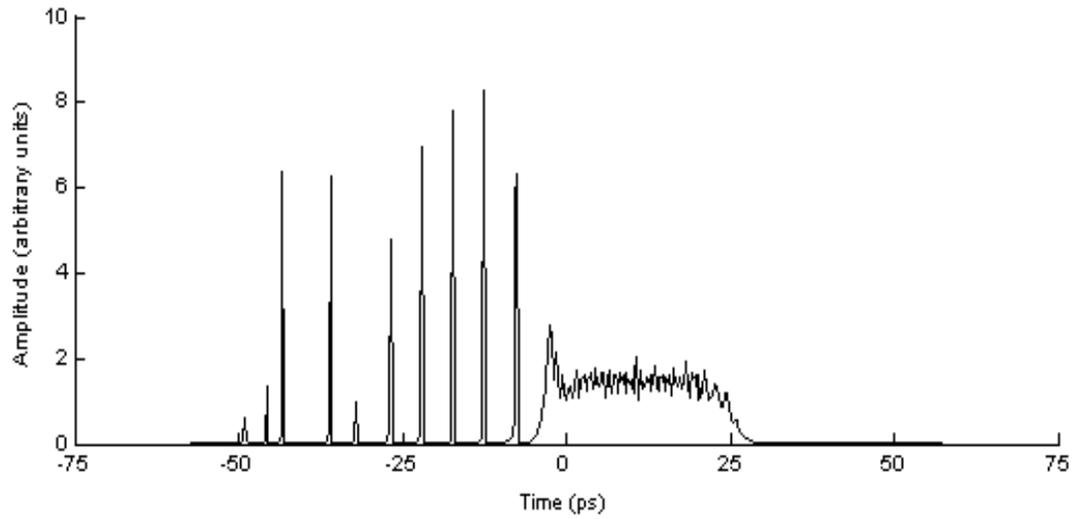
(d)
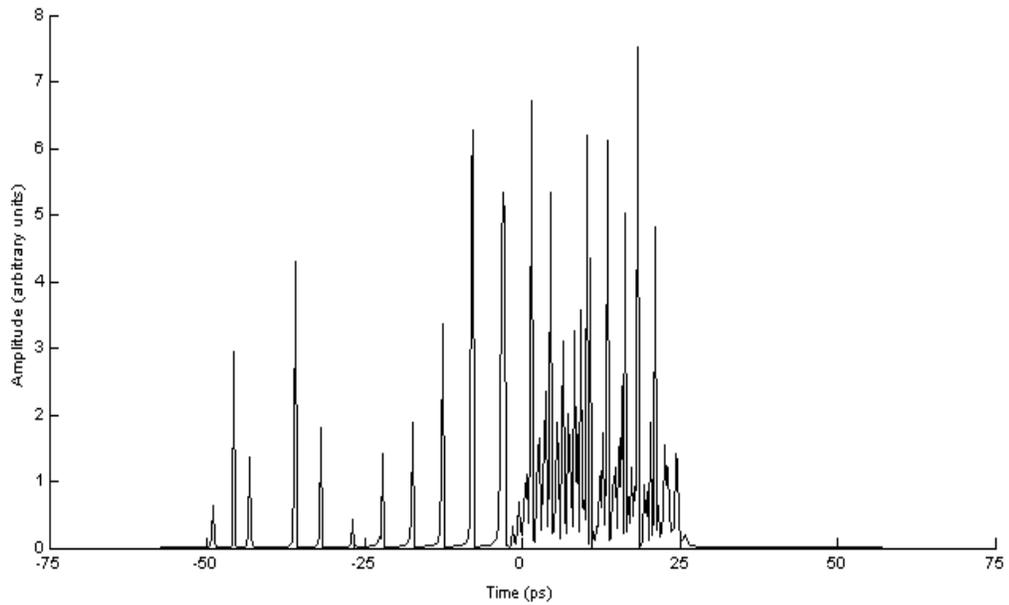
Figure 4.13. Collapse of 500 MW pulse at (a) 50 cm, (b) 70 cm, (c) 75 cm, and (d) 80 cm. The pulse has propagated over a longer distance before the model fails because the initial intensity resulted in smaller collapse peaks on the trailing edge, which delays the collapse of the pulse.

The reasoning behind the formation of these collapse events on the trailing edge of the pulse is not known. Because they emerge only after the pulse has collapsed significantly on the leading edge, and because they grow concurrently from the trailing edge instead of breaking off of the main body of the pulse one at a time, they could be the result of the code no longer modeling the pulse accurately due to the field moving off of the boundaries of the frequency grid used to store the field. This means that there are non-zero values of the field that have moved past the boundaries of the grid and have wrapped around to the other side of the grid, which invalidates the model.

The large number of very intense collapse events on the leading edge of the pulse could lead to the field moving off of the grid, which would no longer allow the model to continue to correctly propagate the pulse. This overflow occurs because the collapse events are so intense and closely spaced that the code begins to generate artifacts, or noise on the empty portions of the grid. Because the collapse events form solely along the leading edge of the pulse, the noise is restricted to one end of the pulse at first, but as more and more collapse events form, this noise begins to appear in all the empty portions of the grid, and the larger artifacts on the leading edge begin to appear near the trailing edge as well. This could lead to additional numerical errors on the opposite end of the pulse as the non-zero values wrap around the grid and affect the portion of the grid where the remaining uncollapsed edge exists. The errors also accumulate on the flat, uncollapsed portion of the pulse but are less evident initially because the uncollapsed portion is not changing in amplitude rapidly like the trailing edge. Eventually the errors on the flat portion act as noise and contribute to the inherent modulational instability of the pulse, causing a rapid collapse of the entire pulse. As more and more collapse peaks

grow on the trailing edge, the model breaks down more with every iteration of the code and eventually the pulse breaks down into a series of collapse events after only a short period of time, as shown above in Figure 4.13. This is not a collapse due to physical means; it is a collapse due to numerical issues with the representation of the field on the grid in the frequency domain. The errors begin to accumulate, and then begin to seed the modulational instability of the pulse, so it is as if the pulse had been seeded with noise initially and the pulse is not only collapsing on its leading edge, but also all along the remaining pulse profile due to this new noise.

If the model is failing in this manner, the plasma generated at the rear of the pulse is not dictating the spacing of the collapse events; rather the collapse events due to accumulating errors in the code are dictating the plasma generation to coincide with the collapse peaks on the trailing edge of the pulse. The collapse event spacing is still controlled by the plasma decay rate.

By studying the representation of the pulse in frequency space, it is possible to see the pulse begin to move off of the edges of the grid, causing the model to no longer accurately portray the pulse in real space. Figure 4.14 shows the progression of a 500 MW pulse off the edges of a 256 element grid in frequency space. The more collapse peaks that are present, the more rapidly the pulse overflows the grid boundaries because errors are generated more rapidly as well. This could explain why the trailing edge collapses are evident sooner on a pulse with higher initial power, because a higher power pulse generates collapse events more rapidly. The higher power pulse, while collapsing at the same rate on its leading edge as a pulse with lower initial power, generates more collapse events within the same amount of pulse consumption. This leads to the model

breaking down more rapidly than the lower power pulse, which requires more time to generate the number of collapse events required to overflow the grid.

Additional experiments were conducted to determine the effect of grid size on the trailing edge collapse. A 500 MW pulse was propagated using both 256 and 512 temporal element grids, while retaining the same time step size. This caused the 512 element grid to be only half as full of pulse information as the 256 element scenario. By introducing this empty grid space, the pulse had more room in the frequency domain before it began to overflow the area taken up by the initial pulse. Therefore, the errors would not begin to wrap around until after the pulse had propagated further. Figure 4.15 shows this delayed progression off of the grid with a pulse with an initial power of 500 MW and a 512 temporal element grid when compared to the 256 element grid used in Figure 4.14. The results suggest that by utilizing a smaller percentage of the available temporal grid space to describe the profile of the initial pulse, the pulse can propagate farther before the errors in the code manifest themselves on the trailing edge of the pulse.

The exact mechanic causing the errors to be generated is still unknown. Possible sources include ringing in the FFT, which would generate additional information on the edges of the pulse in the frequency domain, and lead to inconsistencies in the spatial representation as well. There may also be an inherent inability of the code to deal with the multiple intense, closely spaced collapse peaks that form on the leading edge of the pulse, which could also lead to artifacts or errors in the pulse propagation. As discussed earlier in the section on time convergence, adjusting the loss terms within the model allow convergence to occur, which could also alleviate the overflow of the grid. This area is an issue that should be covered more in future work.

(a)

(b)

66
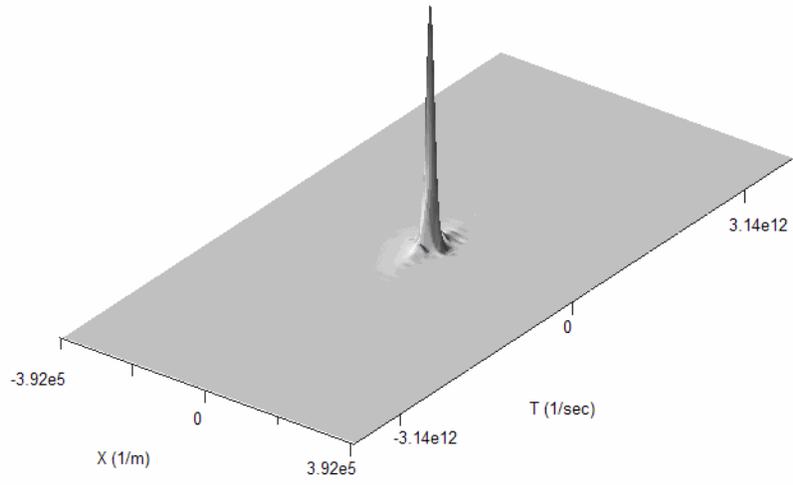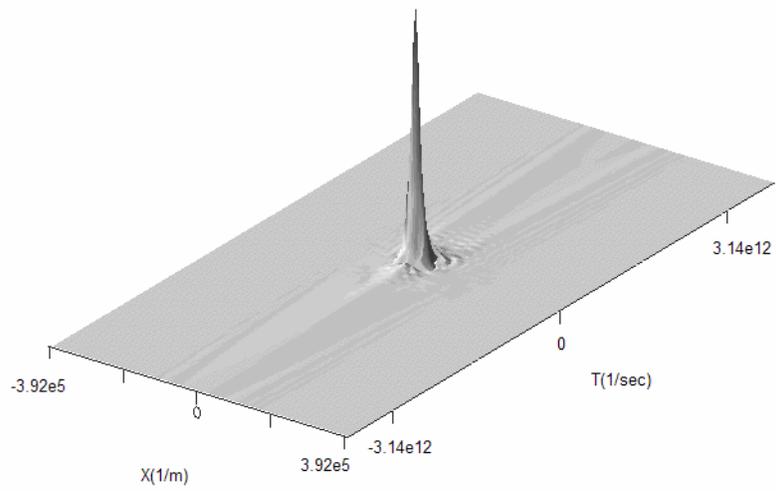
(c)
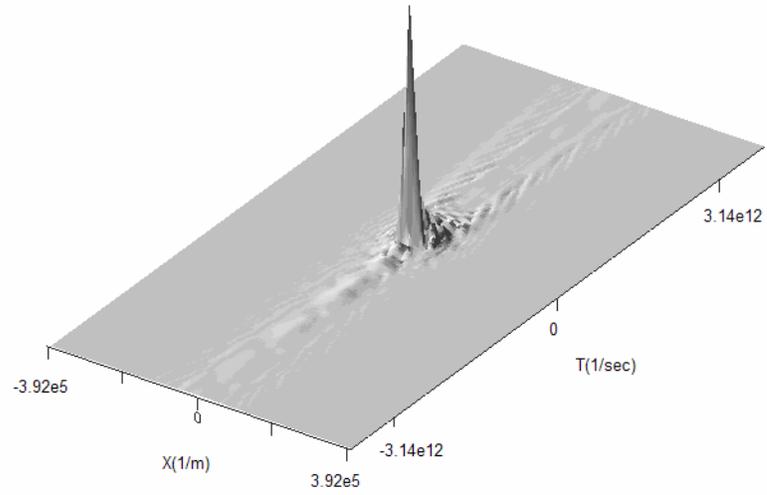
(d)
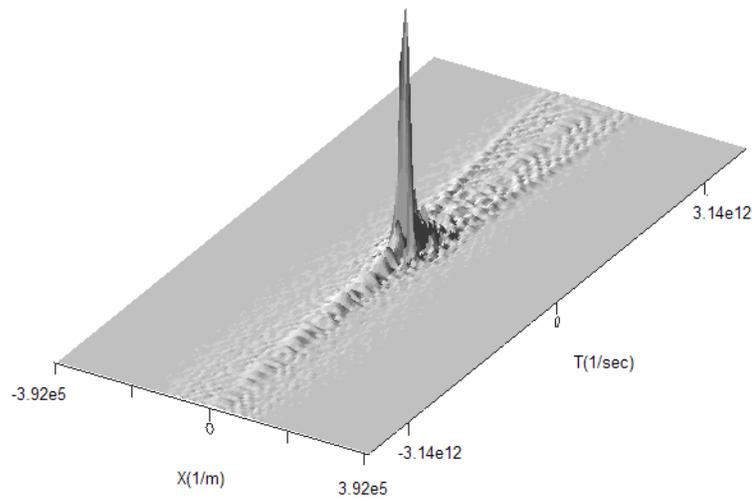
**Figure 4.14.** Progression of a 500 MW pulse off of a 256 element grid in the frequency domain at (a) 5 cm, (b) 15 cm, (c) 25 cm, and (d) 50 cm.

(a)
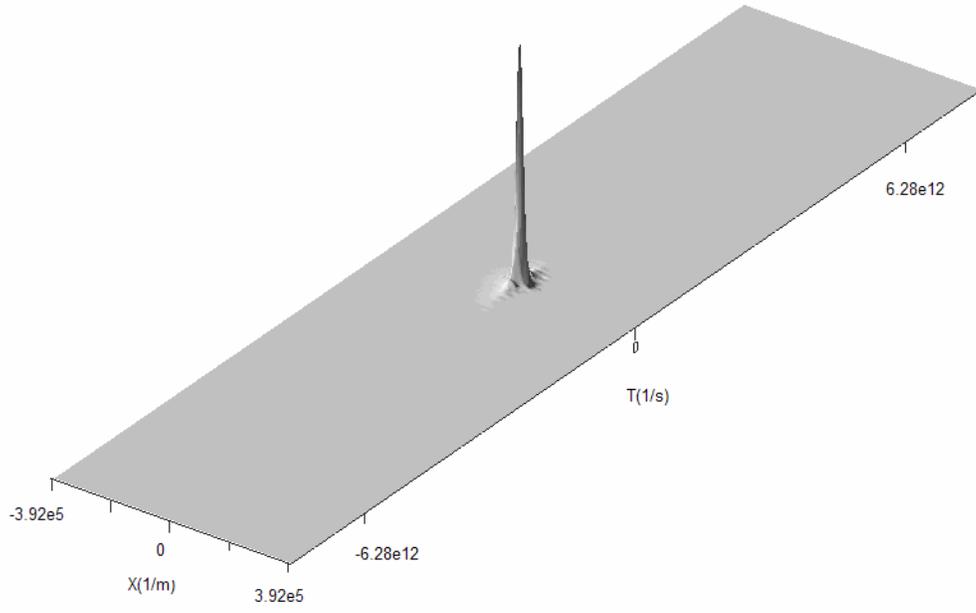
(b)
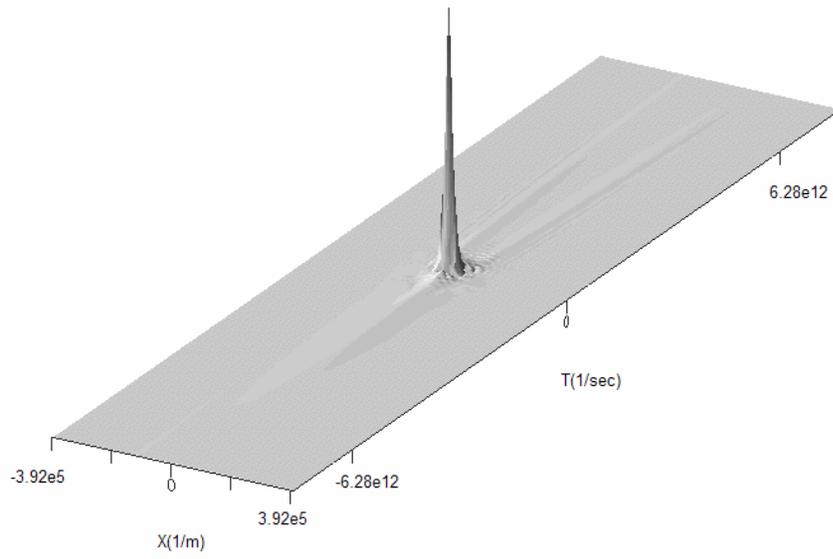
(c)
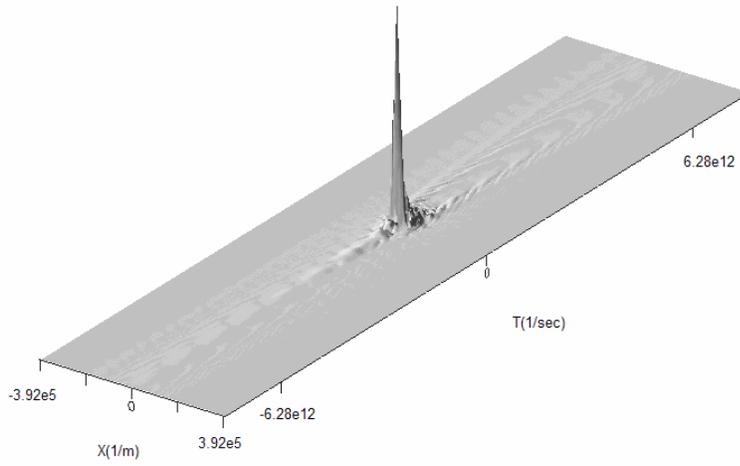
(d)
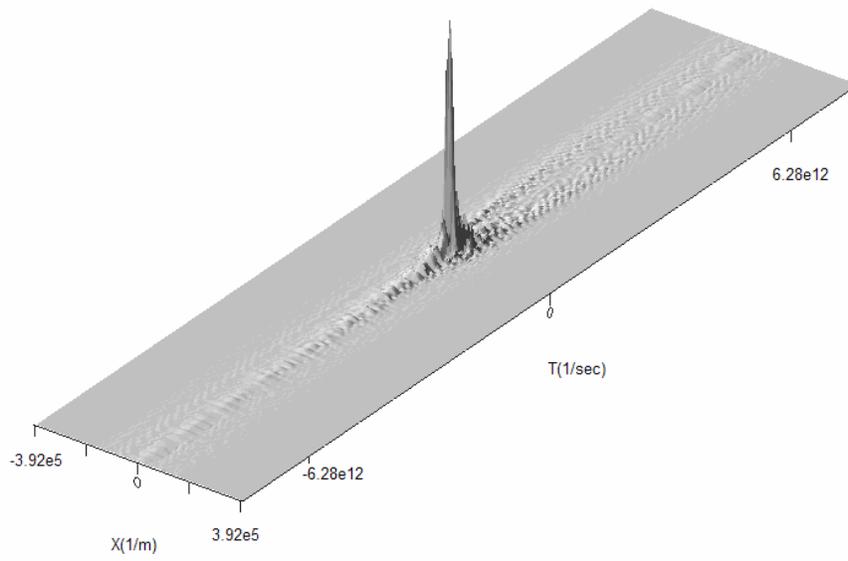
Figure 4.15. Progression of 500 MW pulse off of a 512 element grid in the frequency domain at (a) 5 cm, (b) 15 cm, (c) 25 cm, and (d) 50 cm.

The spacing of the collapse peaks on the leading edge of the pulse was due to the decay rate of the plasma, so the electron-positive ion recombination coefficient α was varied to determine what effect this had on the spacing or formation of the collapse peaks. The pulse was very sensitive to changes of α, so only slight adjustments were made. Changing the value of α to 1.5×10^{-12} m^3/s and 0.7×10^{-12} m^3/s resulted in very different propagation profiles when compared to the nominal value of 1.1×10^{-12} m^3/s. Figure 4.16 illustrates the changes due to varying α.

Higher values for α resulted in more peaks being generated as the plasma decayed faster, allowing the front of the pulse to begin a new collapse sooner. A lower decay rate led to fewer collapses on the leading edge of the pulse and also an overall higher amount of plasma existing in general, which caused the main body of the pulse to be reduced in amplitude. Varying α produced results very similar to that of changing the initial peak power of the pulse. A lower α was similar to a lower initial peak power, and a higher α produced a result much like that of a pulse with a higher initial peak power. An additional observation was that the pulse propagation was very sensitive to changes in α. It was not possible to alter it more than $0.5 - 0.7$ m^3/s without causing the model to fail. If α was changed beyond this range, the pulse was able to grow without bounds very rapidly, or was completely damped out within a few propagation steps, which returned invalid results in both cases. This illustrated the delicate balance between the pulse intensity and the defocusing effect of the plasma in pulse propagation.

(a)
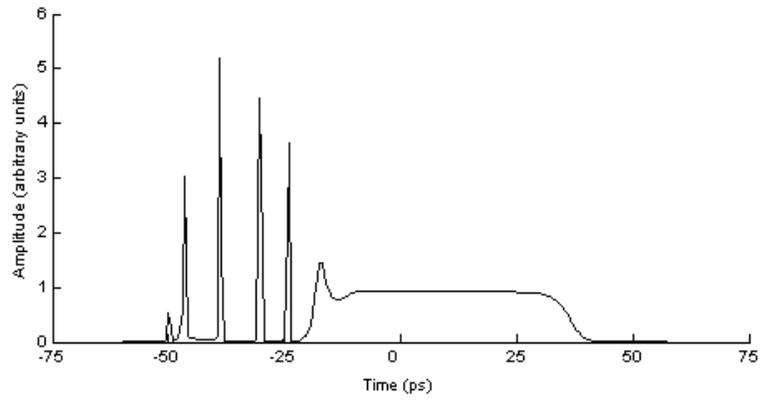
(b)
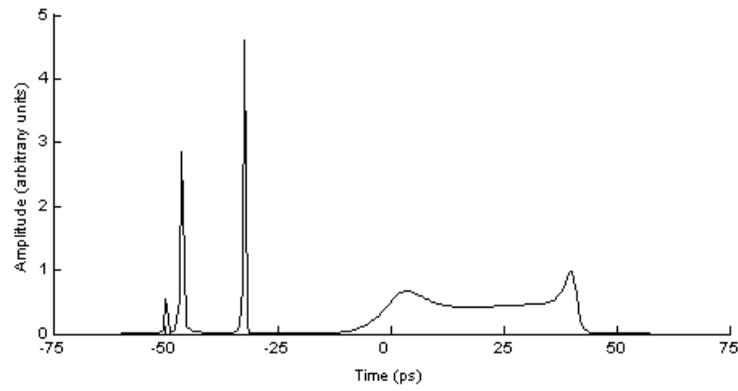
(c)
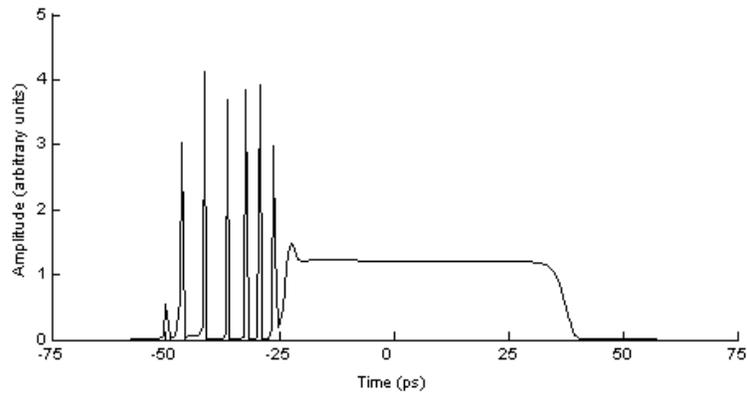
Figure 4.16. Comparison of 1000 MW pulse after 25 cm of propagation with varying alpha values equal to (a) $1.1 \text{ m}^3 / \text{s}$, (b) 0.7 m^3 / s , and (c) 1.5 m^3 / s .

71

Group Velocity Dispersion and Short Pulses

Once the time step convergence had been tested and GVD had been included into the propagation model, short pulses of less than one picosecond in duration were modeled to see how they behaved. This was useful because it is easier to experimentally replicate pulses of these lengths at the intensities required to form filaments. It is hoped that the results of these modeling runs can be experimentally verified or compared to experimental data with the appropriate laser source.

As expected, there were no differences in the longer duration pulses due to the addition of GVD. Initial runs using a GVD value of 2×10^{-28} s/m [20] clearly made no difference in the propagation of long pulses with durations of more than one picosecond. Figure 4.17 shows the pulse propagation of a 100 ps pulse with GVD compared a 100 ps pulse with no GVD term, and a 10 ps pulse with GVD compared to a 10 ps pulse with GVD. As the pulse duration became shorter, GVD did play a role. Figure 4.18 illustrates the effect GVD had on the propagation of a 10 fs duration pulse.

(a)
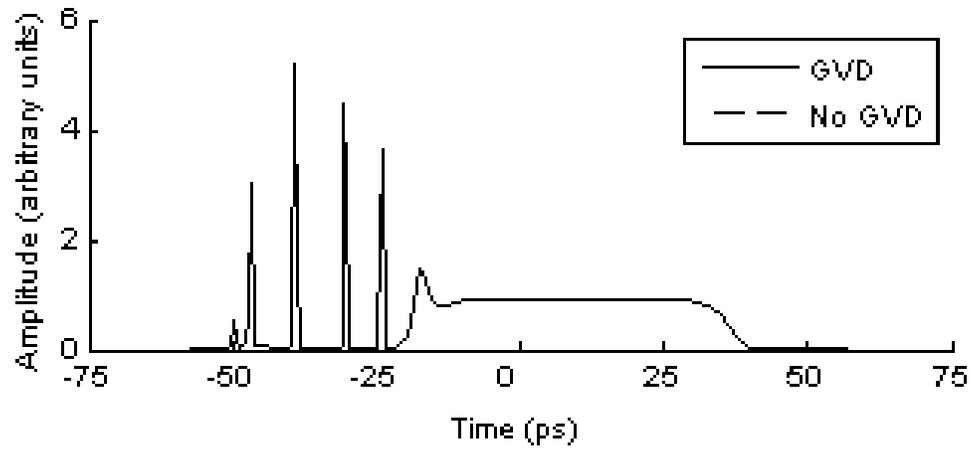
(b)
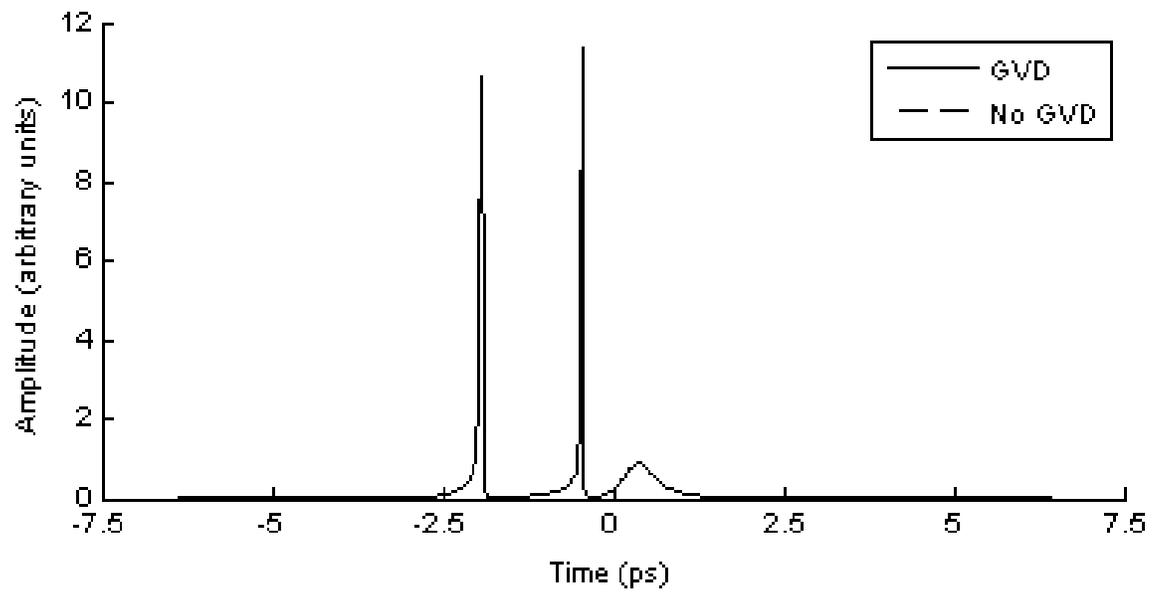
Figure 4.17. Comparison of (a) 100 ps and (b) 10 ps duration pulse propagated over 0.25 m with no loss or GVD to the same pulse with loss and GVD included. There are no differences in pulse profiles.
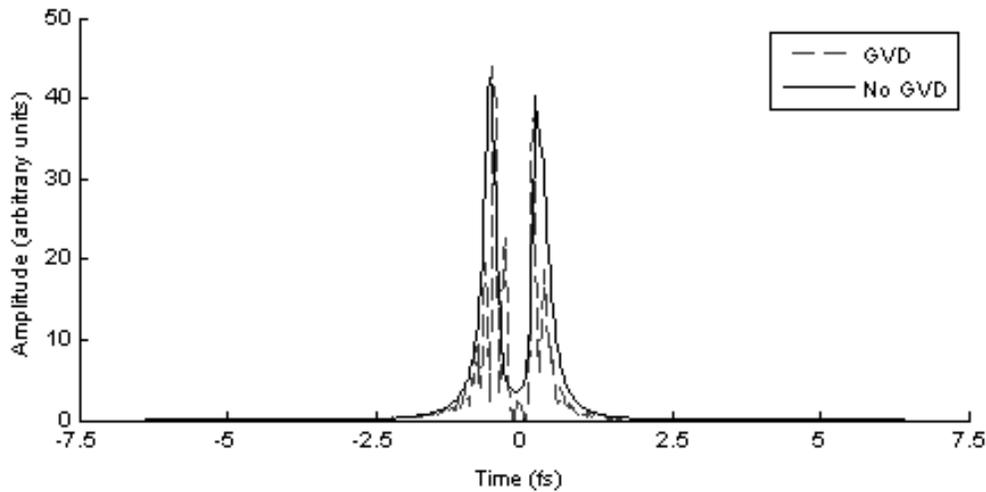
Figure 4.18. Comparison of a 10 fs pulse without GVD to a 10 fs pulse with GVD included. While the overall shape is roughly the same, there are additional collapse characteristics present when GVD is included. The two pulses have propagated a distance of 6 cm.

The first issue was to determine if short pulses on the order of 10 fs would still exhibit collapse events like the ones observed on longer pulses of several picoseconds or more. Using an initial peak power of 500 MW, the pulse would still collapse as it propagated. The shorter pulses collapsed even more quickly than the long pulses because there was less pulse length for the collapse events to act on, so after the first collapse occurred the pulse would quickly die out. The majority of the power was lost to the collapse events, and the rest of the pulse was not intense enough to sustain itself and continue to propagate. With a shorter pulse, only one collapse event was required to consume over half of the pulse, and the same series of events observed in the longer pulses took place to completely destroy what remained of the short pulse. This can be seen in Figure 4.19.

(a)
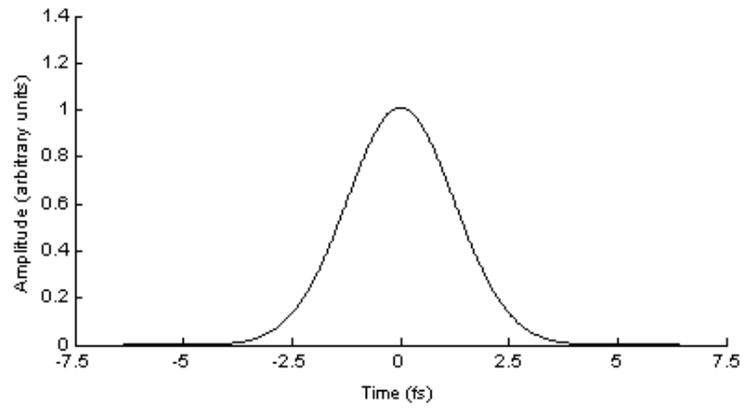
(b)
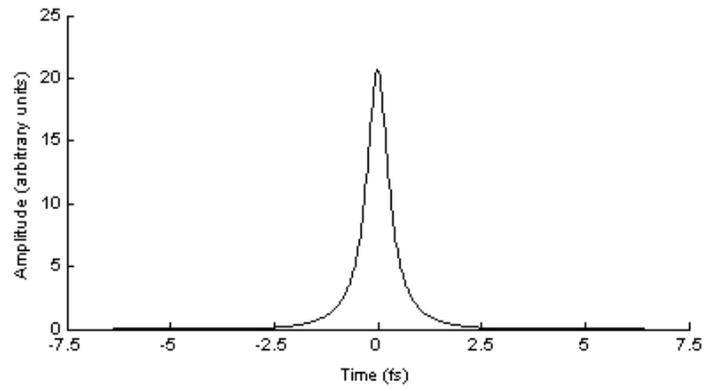
(c)
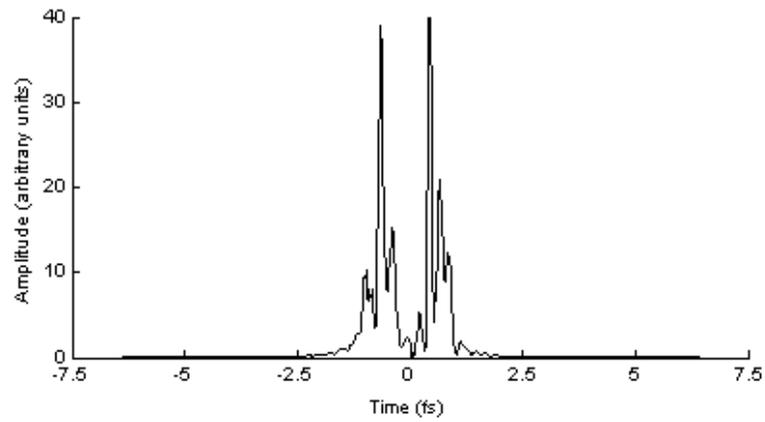
Figure 4.19. 10 fs pulse at various stages of collapse after (a) 0.5 cm, (b) 5 cm, and (c) 7.5 cm of propagation.

Because the 10 fs pulse still collapsed, the initial peak power was reduced to one critical power. The longer pulses would still collapse at lower powers, but the total collapse was delayed because the collapse of the trailing edge occurred after the pulse had propagated a longer distance. The question remained whether this was also the case in the short pulse regime. Reducing the initial power to 125 MW, another run was made to see if the pulse would still collapse. As in the case with the 500 MW pulse, the collapse still occurred but over a longer time period as the collapse event took longer to resolve itself from the main body of the pulse. Instead of breaking into separate peaks, the pulse slowly intensified until it reached peak intensity, and then dropped in amplitude before the multiple peaks became apparent. Therefore, even when reducing the power to one critical power, the shorter pulses could not find the balance needed to propagate without collapsing and breaking down totally. Several additional initial powers were tested to observe the manner in which the pulse would collapse in each case. The results were consistent with both the way in which the short pulse would eventually collapse and the behavior exhibited by long pulses collapsing at varying initial peak powers.

The behavior and collapse of short pulses did not demonstrate the possibility of short pulses in the model forming solitons and propagating over long distances. In addition, the individual collapse events on the leading edge of the longer pulses did not exhibit any ability to continue propagation once the longer pulse had been consumed by the collapse of its leading edge. However, this could be partially due to the fact that the model may break down once the leading edge has a substantial number of collapse events present, so any results past this point of propagation would be invalid. In addition, the use

76

of Gaussian shaped pulses rather than hyperbolic secant initial pulse shapes could contribute to the collapse of the short pulses, and merits further investigation.

(a)
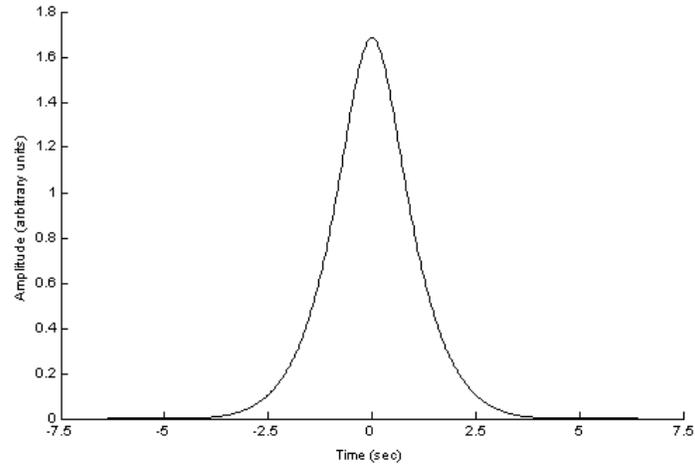
(b)
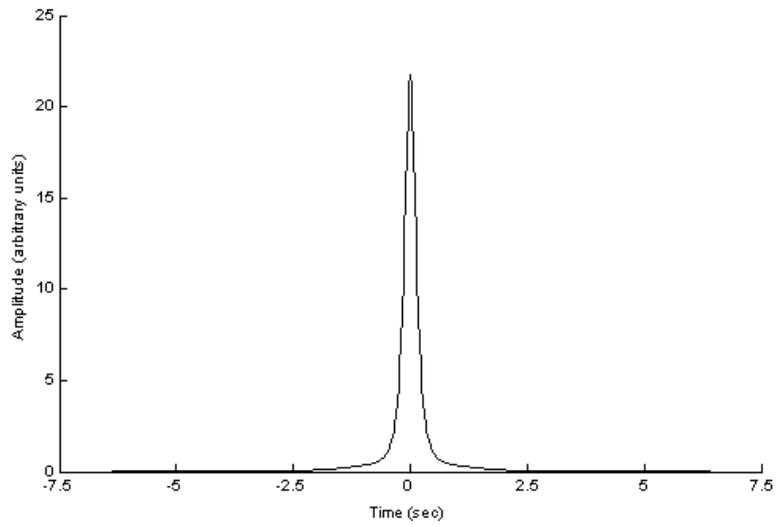
(c)
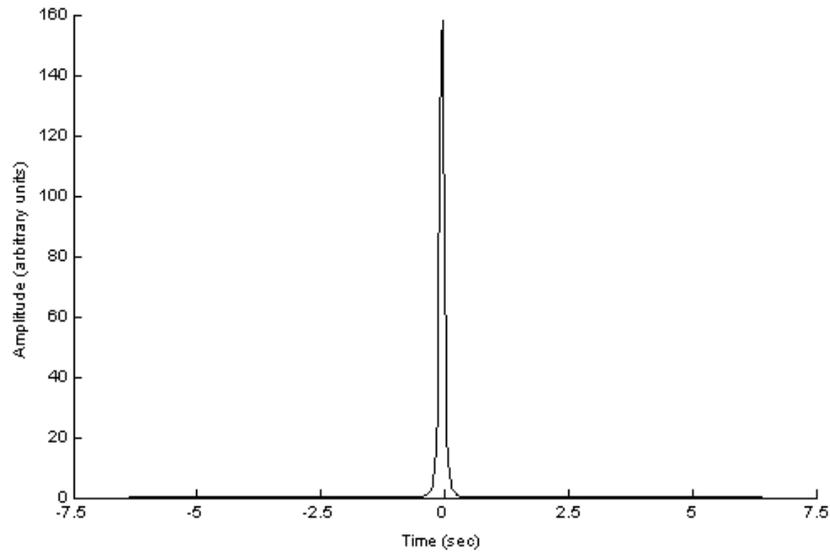
(d)
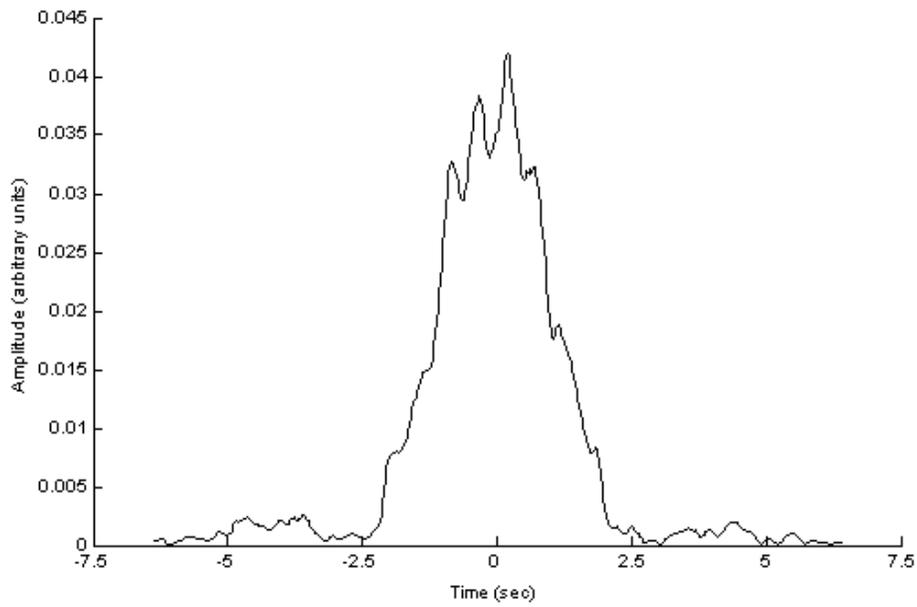
Figure 4.20. 10 fs pulse with 125 MW initial peak power at (a) 10 cm, (b) 25 cm, (c) 35 cm, and (d) 1 m of propagation.

78

Summary

The effects of varying numerical parameters illustrated the importance of capturing as much detail as possible in the modeling of the filament and its propagation. Finer grid and propagation step sizes resulted in more sharply defined collapse events and did not allow for artificially lengthened propagation distances. The optimum combination of 128 spatial elements and 5×10^{-4} m propagation step size resulted in the best results that still allowed for a reasonable computation time.

In the temporal grid, a ratio was determined between the shape of the initial pulse and its duration and the temporal grid size that defined the pulse in the numerical model. The grid size was $1/100^{th}$ of the pulse duration for a supergaussian pulse profile, and $1/20^{th}$ for a Gaussian profile. This was assuming a 512 element temporal grid, which was again the maximum number of elements that still would produce results in a reasonable amount of time. Convergence in the temporal grid was not evident until additional tests were conducted. By altering the loss term β by an order of magnitude (which is within the accuracy that the term is currently known), and using a 250 MW pulse it was possible to show convergence. This suggests that the loss terms in the model need to be carefully studied and adjusted to determine what effect they have on the overall propagation of the pulse, and the other results should be studied again with the adjusted parameters present.

The linear rate of collapse was not dependent on initial peak power. The initial power had no effect on how fast the pulse would collapse overall. However, while studying this issue a number of other behaviors became apparent. First, the number of collapse events that take place within the collapsed portion of the pulse after a certain distance of propagation is dependent on the initial power. Secondly, the peak spacing is

due to the rate at which plasma is generated by the pulse, and the decay rate of the plasma.

The trailing edge of the pulse was also observed to collapse, and the collapse events and plasma related in the same way as they did on the leading edge. However, these collapse events grew at the same rate instead of forming one at a time, and once they formed the pulse would collapse rapidly. The propagation distance at which the trailing edge collapsed decreased with increasing initial power. Additional collapse events could also be distinguished on the remaining flat portion of the pulse, but this was attributed to numerical errors that would grow exponentially once both ends of the pulse collapsed. A possible explanation for why the trailing edge began to collapse is the accumulation of errors due to field overflowing the model's grid in the frequency domain and resulting in the breakdown of the code. The primary reason this occurred was because of the large number of collapse events present in pulses with higher initial peak powers or in lower power pulses that had propagated a further distance, resulting in a larger number of collapse events on the leading edge of the pulse. In addition, by changing the percentage of total grid space used to define the actual pulse, it was possible to delay or lessen the effects of the grid overflow on the trailing edge of the pulse, which would affect the collapse events on the trailing edge as well.

The electron-positive ion recombination coefficient was also adjusted once the relationship between the collapse events and the plasma was determined. Because this coefficient dictated the plasma decay rate, altering it changed the way that the pulse would collapse as it propagated. The results were similar to those obtained by changing the initial peak power of the pulse.

As shorter pulses were investigated, the addition of group velocity dispersion to the propagation model became a necessity. While not affecting the longer pulses, pulses less than 100 fs in duration illustrated effects of GVD when compared to pulses propagated without it. However, the short pulses would still collapse in the same manner as the longer duration pulses, which made the continued propagation of the collapse events seem unlikely. Runs with 100 ps pulses showed no indication that the collapse events would continue to propagate and did not differ from the tests conducted with no GVD present. This could be attributed to the breakdown of the current model in the long pulse tests. Reducing the initial peak power of the short pulses did not significantly lengthen the propagation distance the pulse could travel before collapsing. Possible causes could include the initial pulse shape used differing from that of a fundamental soliton, which is a hyperbolic secant pulse rather than a Gaussian.

V. Conclusion and Recommendations

Chapter Overview

This chapter deals with the overall conclusions that can be drawn from the modeling runs conducted in this work. The previous state of the model and its limitations are reviewed, and the improvements and additional questions resulting from the work accomplished here are summarized. In addition, recommendations for future work building on these results are introduced.

Conclusions of Research

Niday concluded that time independent modeling of long pulse filament propagation in the UV was hindered by two factors: the modulational instability of the pulse due to spatial and temporal perturbations present in the initial field and the transient edge effects of a finite pulse which resulted in the complete collapse of the pulse as it propagated through space [19]. The collapse due to edge effects was further studied in this work in an attempt to prevent or mitigate these destructive effects from occurring. In doing so, several areas were investigated.

First, the numerical parameters of the model were studied to determine if the numerical parameters were not fully capturing the information of the field and causing the pulse to collapse as it propagated. The spatial elements used to define the pulse and the propagation step sizes were adjusted to determine an optimal combination of parameters. The goal was to minimize the time required for the model to propagate a pulse over a set distance but still provide adequate resolution of collapse events as the leading edge of the pulse collapsed. While it was possible to reduce the collapse of the

leading edge of the pulse, this was determined to be caused by a lack of resolution in the numerical spatial grid, and was remedied by using more elements to define the grid along with a smaller propagation step size to capture all the events during propagation. The results of varying propagation step sizes converged at 5×10^{-4} m. The number of spatial elements used throughout the study was 128 and showed a convergence of results when the grid size was increased. The resolution of pulse structure and running the code within the processing and memory constraints of the computer used for the tests were sufficient to duplicate the results of Niday [19].

In addition, convergence of results was studied by varying the temporal step size that defined the time grid. Because the collapse events seemed to condense to a size defined by the temporal grid, a smaller step size was desired to fully resolve the structure of these individual collapses. In the case of the time step size, there were limitations regarding how large the temporal grid could be made due to the processing power and memory of the computer used to run the model. Given any pulse duration, the temporal step size could only be made so small before the field went off of the grid and returned invalid results. Moving to a larger number of elements to define the temporal grid would alleviate this until the step size was again made too small for the grid. However, using a larger grid slowed the model down significantly, and it was not possible to infinitely increase the temporal grid size, so a compromise again had to be made between the resolution gained by utilizing a smaller time step and the loss of efficiency of the model due to using a larger number of time elements. It was determined that depending on the shape of the pulse profile, a ratio of pulse duration to step size would be used in all runs. Additional studies in this area concluded that the MPI coefficient had an impact on how

the pulse propagated. Because the coefficient is not well known to a high degree of accuracy, adjusting it by an order of magnitude was a reasonable variance in its value, and this adjustment along with using a lower power pulse led to the results beginning to converge. Further reducing the time step to an even smaller size would result in complete convergence. However, because the results shown from other areas of investigation such as the structure of the collapse peaks and plasma generation were obtained without this adjusted loss term, future work could include attempting to duplicate these other results with the adjusted loss parameter.

The effect of the initial peak power was studied in an attempt to determine the nature of the collapse events. While Niday [19] calculated that the collapse rate of the pulse was linear, it was found that the initial power had no effect on this linear rate, as all pulses collapsed at the same rate despite varying the initial peak power. However, the initial power did have an effect on the number of collapse events that took place over a given propagation distance. Deeper investigation attributed this to higher initial powers leading to a more rapid formation of peaks on the leading edge of the pulse, and the spacing between these peaks was due to the decay rate of the plasma being created by the collapse events. As the very intense collapse peaks formed, plasma was generated at high levels, damping the peak immediately. The collapse peak would break off from the main body, and a new one would begin to form as soon as the plasma decayed to a level low enough to allow the pulse to intensify once more.

Another area where the initial peak power had an effect was in the formation of collapse events on the trailing edge of the pulse. Once the leading edge had collapsed enough to consume the majority of the pulse, the trailing edge would begin to experience

a rapid and concurrent collapse. Numerical errors would seed the modulational instability of the model and cause collapse structures to exponentially grow out of the remaining flat portion of the pulse. The collapse of the two ends and the modulational instability all contributed to a complete and rapid collapse of the pulse to the point where the model was no longer valid. At this point, the results were invalid as the only information was a series of peaks on the order of the grid spacing. The reasoning behind why the trailing edge would suddenly start to collapse was unknown. A possible explanation is that the field overflows the grid in the frequency domain once a significant number of collapse events are present on the leading edge. This leads to non-zero elements wrapping around to the other side of the grid and causing the model to break down. It also suggests that the larger number of collapse events generated by higher power pulses contribute to the grid overflow and that the model will become invalid more rapidly as the pulse power increases. Lower power pulses are still susceptible to this behavior, but after a longer propagation distance because the pulses must propagate further to generate the required number of collapse events to cause the pulses to break down. Also, by changing the percentage of the temporal grid used to define the pulse – either by increasing the grid size and holding the time step constant used to define the pulse or by increasing the time step size – the collapse of the trailing edge can be delayed or minimized. This points to a relationship between the trailing edge collapse and the grid overflow issue as with a larger temporal grid, the errors have longer to travel before they begin to wrap around grid and affect the trailing edge of the pulse.

Because the electron-positive ion recombination coefficient was one of the factors that controlled the rate of plasma decay, it was varied and its effect on the collapse of the

pulses was again studied. The collapse events on the leading edge of the long pulses were spaced out according to the plasma decay rate. Changing α led to fewer or more collapse events as the plasma decayed more slowly or more rapidly. Also, the more slowly the plasma decayed, the longer it could act on the entire pulse and would cause the pulse to behave as if it was initially created with a lower peak power.

Finally, short pulses were studied to determine if the individual collapse events of the long pulse could continue to propagate with soliton-like behavior. Studies of 10 and 100 fs pulses at varying power levels indicated that these pulses were subject to the same edge effects as the long pulses of hundreds of picoseconds, and were not capable of propagating long distances or exhibiting soliton-like behavior. Additional runs with 100 ps pulses showed no change in the formation or evolution of the leading edge collapse peaks. These peaks did not show any signs of propagating once they had broken apart from the main pulse, which suggested that the individual collapse peaks would not exhibit soliton-like behavior. The initial shape of these short pulses and the collapse events could contribute to the lack of continued propagation, as they deviated from the hyperbolic secant shape required to form a fundamental soliton.

Significance of Research

The benefits of utilizing light filaments in the areas of remote sensing and spectroscopy are of value to the Air Force. Understanding the way that these filaments propagate and the limitations involved in their use is the first step from moving from theoretical simulations to physical recreations of the predicted behaviors, or, alternatively, in providing explanations for experimental results. Robust and detailed

models are required to investigate the usefulness of this region of the spectrum in creating and propagating filaments. Because of the instabilities in the propagation of these long UV pulses detailed by Niday [19], the more that is known about how and why these pulses collapse helps create a deeper understanding about the pulses and a greater possibility of realizing practical uses of UV filaments in Air Force applications.

The fact that the consumption rate of the pulse by the collapse of the leading edge is not linked to the initial peak power of the pulse is promising in that more powerful pulses could be used without fear of an even more premature collapse, leading to more power available on the target of interest. . However, the inability to mitigate the collapse events on the leading edge of the pulse still hinders the distances that these filaments can propagate in the model, which could limit their use in long distance sensing given that the same behavior occurs in an experimental environment. The determination that the spacing of the collapse events is dependent on the initial peak power of the pulse and the plasma decay rate illustrates that the pulse collapse is not an arbitrary phenomenon. There is some structure that can be associated with how the pulse is consumed by the collapse events, and there may be some way to take advantage of this collapse structure to lengthen the distance of filament propagation.

The evidence of a trailing edge collapse is important because it brings to light another possible source of instability in the pulse. Until more is known about the cause of this collapse, however, nothing can be definitively said about its effect on propagation. The possibility that it is a numerical error in the model needs to be investigated to prove that the model is accurately modeling filament propagation, and not contributing to a premature collapse of the long pulse. Additionally, if the collapse of the pulse is

contributing to the breakdown of the model, a numerical solution needs to be found that allows the model to continue to propagate the pulse as the leading edge is consumed by collapse events. Finding flaws in the way that the model propagates the pulse is significant because it allows improvements to be made to the model from which additional information may arise, and may alter previous results in a way beneficial to the long-distance propagation of UV light filaments.

Finally, the addition of GVD to the model adds another layer of capability to the program. The ability to model short pulse propagation is important in studying individual collapse events, the continued possibilities of propagation once the long pulse has collapsed, and the further verification of the code in the IR spectrum by comparing results to published work. Each verification of the numerical model lends strength to the validity of the results obtained in the UV, and the more complex the model is, the more ways exist to study UV filament propagation in a variety of situations.

Recommendations for Future Research

There are still many areas to be investigated regarding long pulse filament formation and propagation in the UV, as well as many ways of expanding the capabilities of the current model. This section covers the known issues that remain unaddressed by the current model, discusses new questions raised by the work done here, and mentions experimental verification that could be of use in future iterations of the model. All topics would be suitable for future work not only to create a more robust and versatile numerical propagation model, but also to continue to study long pulses in the UV accurately.

First, simplifications to the propagation equation still remain. For example, the Raman effect has been neglected here, and could be included in the propagation model to study the results of non-instantaneous self-focusing. Restoring the last term in Equation 2.1 to the model will include Raman scattering in the propagation scheme [29]. This includes the time dependence of the nonlinear refractive index and changes the n_2 term to

$$ik_0 n_2 |\mathcal{E}|^2 \mathcal{E} \rightarrow$$
$$ik_0 (1-f) n_2 |\mathcal{E}|^2 \mathcal{E} + ik_0 f n_2 \left[\int_{-\infty}^{\infty} dt' R(t-t') |\mathcal{E}(t')|^2 \right] \mathcal{E}. \tag{5.1}$$

In Equation 5.1, f is the fraction of the nonlinear response contributed by the time-dependent component. The time-dependent component in this case is stimulated rotational Raman scattering. Plasma diffusion is another physical characteristic that is not taken into account by the current model, and can be included by letting D be nonzero in the plasma equation given by Equation 2.2. For an even more complex and realistic model, adding more refractive index variation terms to the propagation equation such as turbulence or a change in the index of refraction due to altitude may be of interest.

Changing the MPI coefficient β also led to a convergence of results which answered a number of questions about the validity of the model. Because the numerical parameters of the model were no longer dictating how the pulse propagated, there remains a considerable amount of work in reviewing the results obtained without the adjusted loss parameter and how changing β affects these results. Figure 5.1 illustrates two such changes in the results. First, the plasma profile has changed – the separation of the peaks does not appear to be dictated by the plasma decay rate. Also, the grid overflow

issue in the frequency domain has been lessened substantially and possibly eliminated, which would stop the trailing edge of the pulse from collapsing due to numerical errors.

(a)
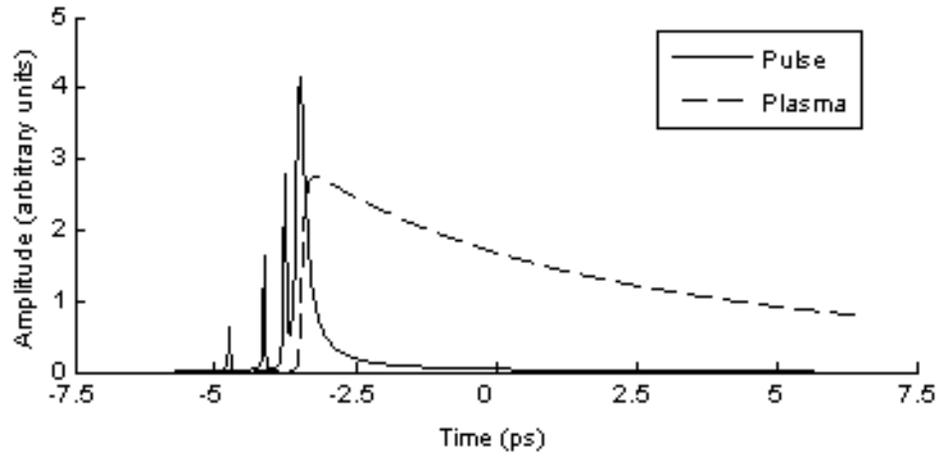
(b)
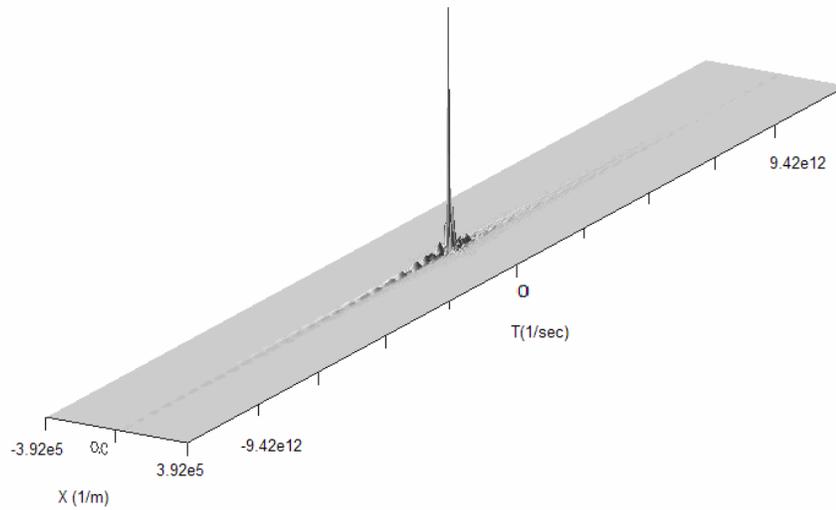
Figure 5.1. Figures showing the (a) plasma profile of a 10 ps, 250 MW pulse after 1 meter of propagation with the increased MPI coefficient, and (b) the same pulse in the frequency domain showing that the grid overflow issue has been greatly reduced or possibly eliminated. Note that in (a) the plasma is not evident in substantial levels between the smaller collapse events, and that the decay time is larger than the pulses looked at previously. The overall effect of changing the value of β needs to be investigated in all of the results in this study.

Specific questions raised from this work are also worth deeper investigation. First, as the pulse is consumed by collapse events on the leading edge, the trailing edge also begins to exhibit features that seem to contribute to the overall collapse of the pulse. What causes this separate set of collapses and why they only form after the pulse has been consumed over much of its length are still unknown. Numerical errors do form on the flat portion of the pulse once both edges undergo collapse. The trailing edge may also be subject to these numerical errors, and those collapse events could simply be another numerical artifact with no real physical meaning. The results shown in Chapter 4 showing the grid overflow in the frequency domain strengthens the argument that the pulse is breaking down due to the large number of very intense, narrow collapse events on the front of the pulse. Alternatively, the pulse could become so unstable from the leading edge collapsing that the trailing edge simply collapses as well, due to uneven areas of the atmosphere or plasma generated by the leading edge. Both physical and numerical reasons behind the collapse of the trailing edge could be an area of study. Also, refining the code to create a more robust numerical model to eliminate any grid overflow issue is also a possibility.

Despite varying numerical and physical parameters in the model, the edge effects continued to collapse and consume the pulse. More work can be done to mitigate or negate these collapse events in an attempt to find a stable, time-dependent long pulse solution. Numerically, one issue that could be investigated is the relationship between the number of elements that define the time grid and the size of the time step. If a way to create a high-resolution time step without having to create a larger time grid could be developed, then greater resolution could be achieved without slowing down the model

with excessive grid size. In addition, one could propagate a long pulse (100 ps) but have enough resolution to closely study the individual collapse events as they emerge from the pulse. Currently, these events collapse down to a size comparable to the grid spacing in the temporal grid with no way of looking at them more closely.

Alternatively, the pulse could be allowed to collapse and the individual collapse events could be studied. The separate pulses that form once the leading edge of the pulse collapses could be remnants of the longer pulse that will continue to fade, or they may be solitons that are capable of propagating long distances after the longer pulse has been completely consumed. This has still not been determined. Modeling runs with multiple short pulses present initially could be conducted to determine this, and also to understand whether these pulses interact with each other as they propagate. The results presented here do not show any evidence of the pulse continuing to propagate once it has collapsed. By altering the propagation model in the ways described above, this may change and is worth pursuing.

The shape of the short pulses and individual collapse events are also important in the formation of solitons. While pulses with peak powers and shapes that do not exactly match the conditions required to form a fundamental soliton are theoretically able to evolve during propagation to match the required parameters, substantial deviations from the ideal parameters could result in a soliton not forming at all [21]. Future studies could include introducing capabilities to the current model to propagate solitons starting with a hyperbolic secant-shaped pulse. Once solitons were modeled correctly, the initial pulse could slowly deviate away from the ideal conditions required for soliton formation and the results studied. This would not only provide a starting point for studying how solitons

92

propagate, but also hopefully provide information on how far the initial pulse conditions can deviate from the required quantities before a soliton does not form. This would help to bridge the gap between an ideal soliton and the types of short pulses and collapse events the model can currently produce, and shed more light on if the collapse events are capable of propagating once the long pulse has broken down into a series of smaller peaks.

The idea of multiple pulses brings up other possibilities. If a long pulse collapses into multiple solitons, forming a pulse train, are these pulses capable of moving through or around obscurants that may be present in the atmosphere, and if so, what effects do these obscurants have on short pulse propagation? The pulses may be able to interact with objects in the atmosphere such as water droplets and reform with little loss in power or even reform into a larger pulse once more. Some studies have already been conducted in the IR testing these theories. Moving these ideas to the UV or continuing the research in the IR is feasible.

If the short pulse model from this work is extended, the model could also become useful for studying pulses in the IR, which require the capabilities added to the model in this work, such as GVD and the ability to model pulses of short durations (10-100 fs). Because a great deal of both theoretical and experimental work has been done in the IR regime, it will be straightforward to compare the results of this model to those achieved by others.

Experimental verification of the collapse of the leading edge of the pulse or consumption of the pulse by modulational instabilities would be useful to evaluate the results predicted by the model. Additionally, experiments involving short pulses in the

UV would be useful to test some of the questions raised above – namely the way in which short UV pulses propagate, or the ability of these pulses to propagate through obscurants or in pulse trains.

Finally, the application of these pulses to areas of interest to the Air Force could also be considered in a survey of current Air Force remote sensing capabilities. Determining the length and wavelength of a filament to be used in activities such as active remote sensing, delivering energy to a target for offensive purposes, or guiding electrical discharges are all topics that could be investigated more closely. The needs of each application as well as the guidelines for wavelength, power and safety are all important when considering possible applications of filament propagation in active Air Force systems.

Bibliography

1. J. Kasparian et al. White-light filaments for atmospheric analysis. *Science*, **301**: 61-64, 2003.

2. P. Rairoux et al. Remote sensing of the atmosphere using ultrashort laser pulses. *Applied Physics B,* **71**: 573-580, 2000.

3. S.L. Chin, et al. Filamentation of femtosecond laser pulses in turbulent air. *Applied Physics B*, **77**: 67-76, 2002.

4. J.H. Marburger. Self Focusing: Theory. *Progress in Quantum Electronics*. **4**: 35-110, 1975.

5. Y.R. Shen. Self Focusing: Experimental. *Progress in Quantum Electronics.* **4**, 1-35, 1975.

6. J. Schwarz, et al. Ultraviolet filamentation in air. *Optics Communications.* **180**: 383-390, 2000.

7. A. Braun et al. Self-channeling of high peak-power femtosecond laser pulses in air. *Optics Letters.* **20**: 73, 1994.

8. E.T.J. Nibbering et al. Conical emission from self-guided femtosecond pulses in air. *Optics Letters.* **21:** 62-64, 1996.

9. R. W. Boyd, *Nonlinear Optics.* Academic Press, New York, 1992.

10. P. Sprangle et al. Propagation of intense short laser pulses in the atmosphere. *Physical Review E.* **66**: 1-21, 2002.

11. W. Liu et al. Experimental observation and simulations of the self-action of white light laser pulse propagating in air. *New Journal of Physics*, **6**: 1-22, 2004.

12. S. Tzortzakis et al. Femtosecond laser-guided electric discharge in air. *Physical Review E.* **64**: 057401, 2001.

13. Jean-Claude Diels et al. Lightning control with lasers. *Scientific American.* August, 1997.

14. J. Schwarz and J.C. Diels. UV filaments and their application for laser-induced lightning and high-aspect-ratio hole drilling. *Applied Physics.* **77**: 185-191, 2003.

15. Ph. Rohwetter et al. Filament-induced remote surface ablation for long range laser-induced breakdown spectroscopy operation. *Spectrochimica Acta B*. **60**: 1025-1033, 2005.

16. M. Mjelnek et al. Recurrent femtosecond pulse collapse in air due to plasma generation: numerical results. *Mathematics and Computers in Simulation*. **56**: 563-570, 2001.

17. S. Skupin et al. Interaction of femtosecond light filaments with obscurants in aerosols. *Physical Review Letters*. **93**: 023901, 2004.

18. G. Mechain et al. Organizing multiple femtosecond filaments in air. *Physical Review Letters*. **93**: 1–4, 2004.

19. T.A. Niday. *Stability and Transient Effects in Ultraviolet Filaments*. PhD Dissertation, University of Arizona, 2004.

20. J. Schwarz and J.C. Diels. Analytical solution for uv filaments. *Physical Review A*. **65**: 1–10, 2001.

21. G. Agrawal. *Nonlinear Fiber Optics, 3rd Ed.* Academic Press, San Diego, 2001.

22. Mlejnek M. et al. Moving-focus versus self-waveguiding model for long-distance propagation of femtosecond pulses in air. *IEEE Journal of Quantum Electronics*. **35**: 71–76, 1999.

23. L. Berge. Boosted propagation of femtosecond filaments in air by double pulse combination. *Physical Review E*. **69**: 065601- 065605, 2004.

24. J.T. Verdeyen. *Laser Electronics*, 3rd *Ed*. Prentice Hall, New Jersey, 1995.

25. J. Gaskill. Linear Systems, Fourier Transforms, and Optics. John Wiley and Sons, 1978.

26. V.P. Kandidov, O.G. Kosareva, and S.A. Shlenov. Spatiotemporal instability of an intense subpicosecond laser pulse in gases. *Quantum Electronics*. **27**: 441-444, 1997.

27. J. Satsuma and N. Yajima. *Progress of Theoretical Physics Suppement*. **55**: 284, 1974.

28. S. Tzortzakis et al. Nonlinear propagation of subpicosecond ultraviolet laser pulses in air. *Optics Letters*. **25**: 1270, 2000.

29. J.R. Penano et al. Stimulated Raman scattering of intense laser pulses in air. *Physical Review E*. **68**: 056502- 056518 , 2003.

Vita

Paul Muller was born in Lakewood, Ohio and lived in various towns in Ohio while growing up. He graduated from Wauseon High School and attended Worcester Polytechnic Institute in Worcester, Massachusetts to pursue a Bachelor of Science in Physics. He graduated from college with Distinction and received his commission as a Second Lieutenant in the Air Force from ROTC at the same time. His first assignment was at Wright Patterson Air Force Base, Ohio where he worked as an electro-optic research scientist and program manager in the Electro-Optics Division of the Sensors Directorate, Air Force Research Labs. His duties included testing long-range hyperspectral sensing devices and managing multiple ground sensor programs for DARPA. His next assignment was to pursue his Masters of Physics degree at the Air Force Institute of Technology. He lives with his wife and dog and is headed to Patrick Air Force Base where he will be employed at the Air Force Technical Applications Center and live in an overpriced house. Paul enjoys racing road and mountain bikes, playing guitar in his rock band, restoring his 1965 Chevelle, and playing video games.

REPORT DOCUMENTATION PAGE

1. REPORT DATE *(DD-MM-YYYY)* 24-03-2006	2. REPORT TYPE Master's Thesis	3. DATES COVERED *(From – To)* Jun 2005 – Mar 2006

4. TITLE AND SUBTITLE	5a. CONTRACT NUMBER
A Study of Collapse Events in Ultraviolet Light Filaments Due to Transient Edge Effects	5b. GRANT NUMBER
	5c. PROGRAM ELEMENT NUMBER

6. AUTHOR(S)	5d. PROJECT NUMBER 2005-017
Muller, Paul L., Captain, USAF	5e. TASK NUMBER
	5f. WORK UNIT NUMBER

7. PERFORMING ORGANIZATION NAMES(S) AND ADDRESS(S)	8. PERFORMING ORGANIZATION REPORT NUMBER
Air Force Institute of Technology Graduate School of Engineering and Management (AFIT/EN) 2950 Hobson Way WPAFB OH 45433-7765	AFIT/GAP/ENP/06-12

9. SPONSORING/MONITORING AGENCY NAME(S) AND ADDRESS(ES)	10. SPONSOR/MONITOR'S ACRONYM(S)
Dr. Arje Nachman AFOSR/NM 110 Duncan Ave Suite B115 Bldg 410 Bolling AFB DC 20332-0001 (703)696-8427	11. SPONSOR/MONITOR'S REPORT NUMBER(S)

12. DISTRIBUTION/AVAILABILITY STATEMENT

APPROVED FOR PUBLIC RELEASE; DISTRIBUTION UNLIMITED

13. SUPPLEMENTARY NOTES

14. ABSTRACT
Intense, short light pulses can form filaments capable of propagating kilometers through the atmosphere. This is due to the nonlinear index of refraction of the atmosphere in response to the pulse's high intensity, which creates a self-focusing effect that further intensifies the pulse. This focusing is balanced by the formation of defocusing plasma by the pulse. A split-step propagation model was used to simulate the propagation of these pulses through the atmosphere and investigate the collapse of long ultraviolet pulses of 10-100 picoseconds in duration due to transient edge effects. The structures of individual collapse events in the pulse were characterized. The pulses collapsed linearly, yet independently of the initial pulse power. The number of collapses the pulse undergoes scaled with the initial power, and the plasma decay rate was found to dictate collapse event spacing. Additional collapses on the trailing edge of the pulse were also observed, and may have been created by the pulse field overflowing the grid used to model the propagation. Group velocity dispersion was included to add capabilities to model short pulses in the ultraviolet. Short pulses of 100 femtoseconds or less were observed to collapse in a manner similar to the longer pulses.

15. SUBJECT TERMS
Light Pulses, Optical Properties, Light Transmission, Soliton, Laser, Nonlinear Optics

16. SECURITY CLASSIFICATION OF:			17. LIMITATION OF ABSTRACT	18. NUMBER OF PAGES	19a. NAME OF RESPONSIBLE PERSON Thomas A. Niday, Capt, USAF (ENP)
a. REPORT U	b. ABSTRACT U	c. THIS PAGE U	UU	109	19b. TELEPHONE NUMBER *(Include area code)* (937)255-3636 x4828; e-mail: Thomas.Niday@afit.edu

Standard Form 298 (Rev. 8-98)
Prescribed by ANSI Std. Z39-18